Multi-scale characterization of Developmental Defects of Enamel and their clinical significance for diagnosis and treatment

Sophia Houari, Karen Derocher, Tran Thu Thuy, Thibaud Coradin, Vesna Srot, Peter A van Aken, Hélène Lecoq, Thierry Sauvage, Etienne Balan, Julie Aufort, et al.

Acta Biomaterialia

Multi-scale Characterization of Developmental Defects of Enamel and their Clinical Significance for Diagnosis and Treatment

--Manuscript Draft--

Manuscript Number:	AB-23-898R2
Article Type:	Full length article
Keywords:	Developmental Defect of Enamel; electron microscopy; Nuclear Techniques; Atom Probe Tomography
Corresponding Author:	Sophia HOUARI, DDS, PhD University of Paris PARIS, FRANCE
First Author:	Sophia HOUARI, DDS, PhD
Order of Authors:	Sophia HOUARI, DDS, PhD
	Karen DeROCHER
	Thu Thuy TRAN
	Thibaud CORADIN
	Vesna SROT
	Peter A. Van AKEN
	Hélène LECOQ
	Thierry SAUVAGE
	Etienne BALAN
	Julie AUFORT
	Marco CALEMME
	Nicolas ROUBIER
	Julia BOSCO
	Katia JEDEON
	Ariane BERDAL
	Derk JOESTER
	Sylvie BABAJKO
Abstract:	Developmental Defects of Enamel (DDE) such as Dental Fluorosis (DF) and Molar Incisor Hypomineralization (MIH) are a major public health problem. Their clinical aspects are extremely variable, challenging their early and specific diagnosis and hindering progresses in restorative treatments. Here, a combination of macro-, micro- and nano-scale structural and chemical methods, including, among others, atom probe tomography recently applied on tooth enamel, were used to study and compare MIH, DF and healthy teeth from 89 patients. Globally, we show that DF is characterized by an homogenous loss of mineral content and crystallinity mainly disrupting outside layer of enamel, whereas MIH is associated with localized defects in the depth of enamel where crystalline mineral particles are embedded in an organic phase. Only minor differences in elemental composition of the mineral phase could be detected at the nanoscale such as increased F and Fe content in both severe DDE. We demonstrate that an improved digital color measurement of clinical relevance can discriminate between DF and MIH lesions, both in mild and severe forms. Such discriminating ability was discussed in the light of enamel composition and structure, especially its microstructure, organics presence and metal content (Fe, Zn). Our results offer additional insights on DDE characterization and pathogenesis, highlight the potentiality of colorimetric measurements in their clinical diagnosis and provide leads to improve the performance of minimally invasive restorative strategies.

Laboratoire Physiopathologie Orale Moléculaire
UMRS 1138 - Equipe BERDAL

Paris, France, March 14th, 2023

Dear Professor William R. Wagner,
Editor-in-Chief of Acta Biomaterialia Journal,

Please find appended our manuscript entitled **"Multi-scale Characterization of Developmental Defects of Enamel and their Clinical Implications for Diagnosis and Repair"**
by "Sophia Houari, Karen DeRocher, Tran Thu Thuy, Thibaud Coradin, Vesna Srot, Peter A. van Aken, Hélène Lecoq, Thierry Sauvage, Etienne Balan, Julie Aufort, Marco Calemme, Nicolas Roubier, Julia Bosco, Katia Jedeon, Ariane Berdal, Derk Joester and Sylvie Babajko" which we would like to submit for publication in Acta Biomaterialia Journal that we choose for many reasons listed below.

Our group has been working on dental enamel pathophysiology for more than a decade with investigations on human tooth samples and the generation of rodent models mimicking human developmental defects of enamel (DDE), in particular dental fluorosis (DF) and molar incisor hypomineralization (MIH). These two diseases are widespread throughout the world and are considered major public health concerns due to consecutive tooth loss and altered quality of life of affected people. Based on a clinical trial (ClinicalTrials.gov NCT04704089), our goal was to collect enamel samples from patients affected by DF or MIH both in mild and severe forms (compared to healthy ones) and to systematically characterize them by state-of-the-art techniques, never applied on this material, at different length scales from clinical optical properties to nano-scale structure.
In this present study, we performed a deep characterization of each DDE which allowed us to highlight four major specific characteristics depending on their severity:
1) A specific digital color parameters (*L*a*b** values measured by a spectrophotometer) for each DDE that are distinct from healthy enamel.
2) DF enamel exhibits wide and rough crystallites forming highly porous structures whereas MIH enamel is formed by small crystallites embedded in an organic matrix.
3) A homogeneous decrease in enamel mechanical properties in DF, while an abrupt change in hardness in the middle third of the enamel was systematically observed in MIH
4) A similar chemical concentration profile across enamel crystallites in both DDE that varies according to the severity of the DDE.
All these characteristics are discussed in the light of the pathogenesis to pave the ground for improved diagnosis and adapted specific treatments.

We selected Acta Biomateriala Journal to submit our original results because it seems the most appropriate to communicate them to researchers, clinicians and engineers who read it. Our data defining the physico-chemical signature of each DDE would not only allow to better understand potential causative factors but also give indications for their therapies and setting new materials up allowing to propose an appropriate care protocol depending on the type of hypomineralization.

We thank you in advance for your interest in our data that we hope suitable for publication in Acta Biomaterialia Journal.

We look forward to hearing from you in due course.

Dr Sophia Houari

Centre de Recherche des Cordeliers – UMRS 1138 – Equipe BERDAL – Université Paris Cité - INSERM
Laboratoire de Physiopathologie Orale Moléculaire
Escalier E - 2è étage gauche- 15 rue de l'Ecole de Médecine - 75270 Paris Cedex 06, Tél. : 01 44 27 55 89

Statement of significance

Developmental Defects of Enamel (DDE) are associated to caries and tooth loose affecting billions of people worldwide. Their precise characterization for adapted minimally invasive care with optimized materials is highly expected. ~~Here~~ In this study, first we propose the use of color parameters measured by a spectrophotometer as a means of differential clinical diagnosis. Second, we have used state-of-the-art techniques to systematically characterize the structure, chemical composition and mechanical ~~optical~~ properties of ~~dental~~ enamel ~~teeth~~ affected by two major DDE, Dental Fluorosis (DF) or Molar Incisor Hypomineralization (MIH). We evidence specific enamel structural and optical features for DF and MIH while chemical modifications of the mineral nanocrystals were mostly correlated with lesion severity. Our results pave the way of the concept of personalized dentistry. ~~In the light of our results, we propose a new means of clinical diagnosis for an adapted and improved restoration protocol for these patients.~~

Response to Reviewer 2

Editor: We still have a few minor items we would like you to address:
1) Figure S4, "MIH" series: correct "deep" to "depth" and the text in the caption from "others" to "other".
2) Figure S2, caption: correct "this three areas" to "these three areas".
We thank the Editor for his detailed reading and for pointing out these errors. All the corrections were made on the Figures S2 and S4 of the supplementary material, as requested.
3) Submit a separate file in an editable file format, such as Word, containing the figure captions for the main figures.
Done
4) Graphical Abstract - increase the font size: (i) the text/labels in the chart is still far too small and (ii) the text in the "HAADF-STEM" image is still too small.
Done

Reviewer #3: In my original review of the initial version of the "Multi-scale Characterization of Developmental Defects of Enamel and their Clinical Implications for Diagnosis and Repair" manuscript I raised 4 main concerns:
1) connecting the material analysis results to the statements on material changes and the colorimetric method
2) connecting, comparing and discussing the observed discrepancies between the various analysis
3) explaining how relevant choices were made during the experiments
4) giving an honest discussion of the limitations of the work

The authors have, in my opinion satisfactorily, addressed 1, 2 and 4 in this new version of the manuscript. Unfortunately, number 3 was only addressed in the letter to the reviewers and even in that response the authors partially argue with their experience. This seems to be a bit of a misunderstanding of the motivation for the criticism. I am not doubting the authors experience, I am worried about reproducibility. Given the large number of potential choices for regions of interest due to the orders of magnitude differences in volumes covered by the various analysis method I would consider it to be exceedingly hard if not impossible to reproduce the authors results based on the information given in the current version of the manuscript. Given that reproducibility is a cornerstone of scientific work, I think it is fair to expect from the authors to provide the necessary guidance/criteria they use to choose regions of interests for the various analysis method either in this manuscript/SM or clearly reference previous work that provides this information.
We thank the Reviewer for his/her suggestions which we find judicious. We add some additional details in the methods part (section 2.2: “Patient recruitment and dental enamel samples selection and collection”) to convince the Reviewer and the readers of the reproducibility of our data: We detailed the criteria we used to choose the regions of interest and harvest them. We insist on the fact that there was no specific selection of the samples prior analyses using a given technique. However, for the tooth enamel surface analysis using techniques like PIGE/PIXE or HR-TEM, we selected only pathognomonic lesions (i.e. a clinical sign that appears only in the context of a specific disease) : the striated pattern with alternating light and dark brown bands that characterize dental fluorosis, or delimited opacities on the first permanent molars or incisors in case of MIH.

Another subtle misunderstanding seems to arise from my criticism of the relation between imaged features and the underlying DDE condition. The authors argue that the clinicians made the right diagnosis. I am not doubting that. My inquiry is more towards getting a judgement from the authors if the specific observed features in a small-/micro-/nano-scale can be uniquely linked to the respective conditions. I'll try to clarify with 2 hypotheticals based on the TEM analysis in Fig. 3:
1) If the authors would be handed TEM lamellae from a human tooth and see the features observed in Figure 3d would they be confident that the tooth is affected by DF without looking at the rest of the tooth?
Yes, we confirmed that the specific observed features in small-/micro- nano scale are specific to each pathology.

The striated pattern observed in figure 3D is pathognomonic to dental fluorosis, meaning this optical observation cannot be seen in any other enamel pathology, neither MIH nor caries or genetic pathologies. We are thus confident that the tooth is affected by DF without looking at the rest of the tooth.

2) If the authors were to be handed a tooth affected by DF, would they be confident that they can find the feature shown in Figure 3d somewhere on the tooth?
No, this pathognomonic sign is not found in all DF but if a striated pattern is found then the diagnosis of DF is certain. That's why a systematic and careful analysis is necessary. Not finding a pathognomonic sign of a pathology doesn't allow to make a diagnosis of exclusion.

Similar hypotheticals could be constructed for other observations, like the changes in enamel hardness, the porosity of crystallites, widening of interrod gaps etc.
Note that I consider it perfectly acceptable that such judgements can't be made for some or even all of the observations made here given the current state of knowledge. I would consider it a notable improvement of the manuscript tough if the authors contextualize their results in a way that allows the reader to comprehend how the authors themselves judge the correlations between nanoscale features and macroscale pathologies identified in their own research.

Contrary to DF exclusively due to excessive fluoride, MIH is the result of multiple factors, none of which is truly causal (https://doi-org.ezproxy.u-paris.fr/10.1007/s40368-021-00646-x. https://doi-org.ezproxy.u-paris.fr/10.1111/cdoe.12229) with more heterogeneous defects, but we found ultrastructural, mechanical and molecular signatures in all our samples without exception, although our sampling is admittedly small:
- Rough and large enamel crystallites signify DF, while the amorphous organic layer hiding the prismatic enamel ultrastructure signs MIH.
- Weak mechanical properties deep in the enamel sign MIH, whereas reduced hardness of outer enamel layer is the sign of DF
- The presence of a clear amide band on the FTIR spectrum is the signature of severe MIH.
Moreover, we highlight that:
- High Fluoride content has been reported in DF (in many studies). Here, we also found high fluoride content in some MIH samples.
- Interestingly, Fe and Zn were found in both pathologies which is a characteristic of lesional enamel.
Thus, despite the different scales of analyses, the five features cited above as a whole sign a DDE. As for the striated pattern that signs DF, not finding such pathognomonic signs doesn't allow to make a diagnosis of exclusion.
We added these points in the discussion of the revised manuscript.

In addition, there are a few small issues I think the authors should check:
1) Atom Probe was developed in the second half of the 1960s [1], so I wouldn't consider it "recently-developed".[1] https://doi.org/10.1063/1.1683116
We thank the Reviewer for the reminder, we modified this claiming in the abstract accordingly.
2) As best I can tell the cross-references to the supplementary figures are off. For example, the "2D and radially integrated diffraction patterns" are in Figure S4 and not Figure S5 in the SM I got.
It seems that the Reviewer didn't have the last version of SM document. We double-checked the indentation of all figures cited in the text and in the document "SM review 2".

Graphical Abstract

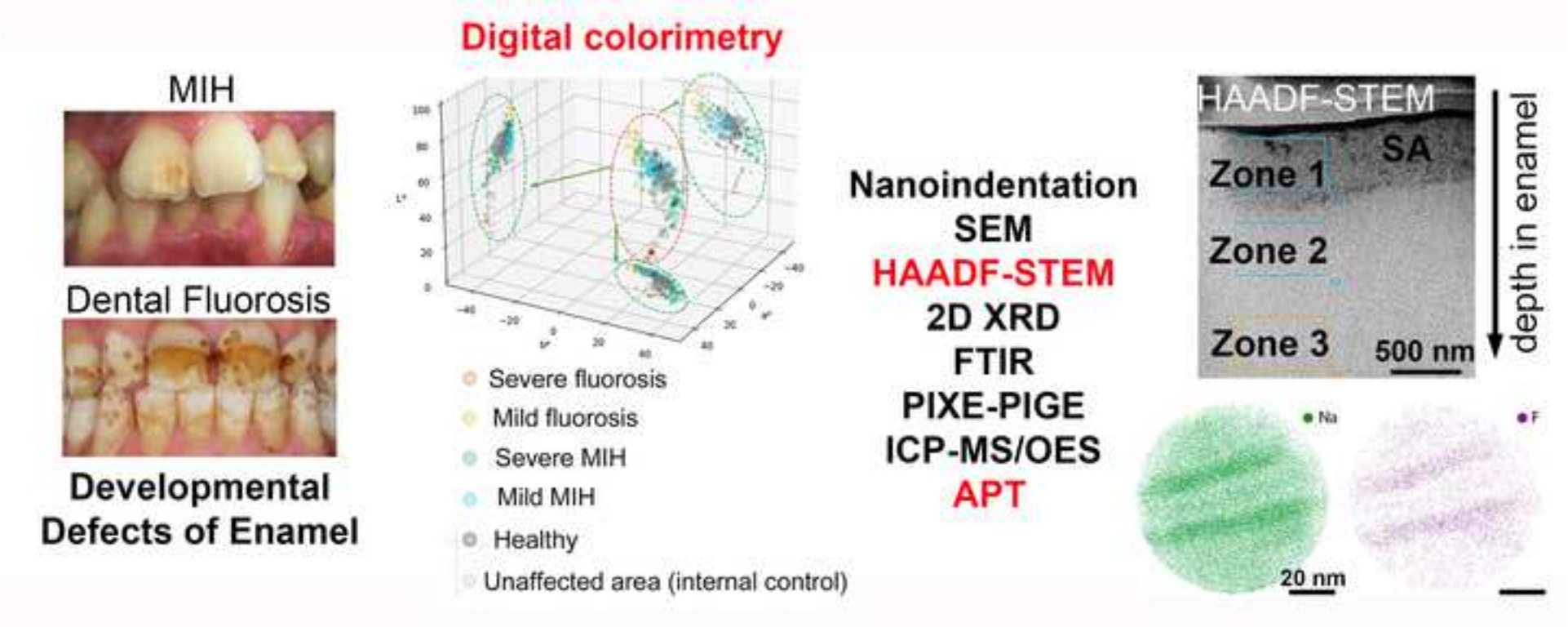

Multi-scale Characterization of Developmental Defects of Enamel and their Clinical significance for Diagnosis and Treatment

Sophia Houari[a,b,c,*], Karen DeRocher[d], Tran Thu Thuy[e], Thibaud Coradin[f], Vesna Srot[g], Peter A. van Aken[g], Hélène Lecoq[h], Thierry Sauvage[h], Etienne Balan[i], Julie Aufort[i], Marco Calemme[j], Nicolas Roubier[k], Julia Bosco[b], Katia Jedeon[a,c], Ariane Berdal[a,c], Derk Joester[d] and Sylvie Babajko[a,c,l].

[a]Centre de Recherche des Cordeliers, INSERM UMRS 1138, Université Paris Cité, Sorbonne Université, Laboratoire de Pathophysiologie Orale Moleculaire, Paris, France.

[b]Unité de Formation et de Recherche d'Odontologie, Université Paris Cité, Service d'Odontologie - Hôpital La pitié-Salpetrière, APHP, Paris, France.

[c]Fédération Hospitalo-Universitaire DDS-ParisNet, INSERM, Université Paris Cité, Assistance Publique-Hôpitaux de Paris, France.

[d]Department of Materials Science and Engineering, Northwestern University, Illinois, USA.

[e]Faculty of Odonto-stomatology, HochiMinh University of Medicine and Pharmacology, HôchiMinh Ville, Vietnam.

[f]Sorbonne Université, CNRS, Laboratoire de Chimie de la Matière Condensée, Paris, France.

[g]Max Planck Institute for Solid State Research, Stuttgart Center for Electron Microscopy, Stuttgart, Germany.

[h]CNRS UPR3079, Université d'Orléans, Conditions Extrêmes et Matériaux: Haute Température et Irradiation, Orléans, France.

[i]Sorbonne Université, CNRS, Institut de Recherche pour le Developpement, Museum National d'Histoire Naturelle, Institut de Minéralogie, Physique des Matériaux et Cosmochimie, Paris, France

[j]Dental Monitoring Company, Paris, France.

[k]CNRS, Centrale-Supélec, Université Paris-Saclay, Laboratoire de mécanique Paris-Saclay, Châtenay-Malabry, France.

[l]UR2496, Biomedical research in Odontology, Université Paris Cité, Montrouge, France.

* **Corresponding author**: Dr Sophia Houari, 15 rue de l'école de médecine, 75006 Paris
Tel :+33612168835. Email adress: sophia.houari@u-paris.fr.

Karen DeROCHER : kaderocher@gmail.com,
Thu Thuy TRAN : tranthuthuyrhm@yahoo.com,
Thibaud CORADIN : thibaud.coradin@upmc.fr,
Vesna SROT : v.srot@fkf.mpg.de,
Peter A. Van AKEN : p.vanaken@fkf.mpg.de,
Hélène LECOQ : helene.lecoq@cnrs-orleans.fr,
Thierry SAUVAGE : thierry.sauvage@cnrs-orleans.fr,
Etienne BALAN : etienne.balan@sorbonne-universite.fr,
Julie AUFORT : julie.aufort@sorbonne-universite.fr,
Marco CALEMME : marco.calemme@gmail.com,
Nicolas ROUBIER : nicolas.roubier@centralesupelec.fr,
Julia BOSCO : julia.bosco@univ-paris-diderot.fr,
Katia JEDEON : jedeonkatia@yahoo.com,
Ariane BERDAL : ariane.berdal@u-paris.fr,
Derk JOESTER : d-joester@northwestern.edu,
Sylvie BABAJKO : sylviebabajko@gmail.com

Abstract

Developmental Defects of Enamel (DDE) such as Dental Fluorosis (DF) and Molar Incisor Hypomineralization (MIH) are a major public health problem. Their clinical aspects are extremely variable, challenging their early and specific diagnosis and hindering progresses in restorative treatments. Here, a combination of macro-, micro- and nano-scale structural and chemical methods, including, among others, atom probe tomography recently applied on tooth enamel, were used to study and compare MIH, DF and healthy teeth from 89 patients. Globally, we show that DF is characterized by an homogenous loss of mineral content and crystallinity mainly disrupting outside layer of enamel, whereas MIH is associated with localized defects in the depth of enamel where crystalline mineral particles are embedded in an organic phase. Only minor differences in elemental composition of the mineral phase could be detected at the nanoscale such as increased F and Fe content in both severe DDE. We demonstrate that an improved digital color measurement of clinical relevance can discriminate between DF and MIH lesions, both in mild and severe forms. Such discriminating ability was discussed in the light of enamel composition and structure, especially its microstructure, organics presence and metal content (Fe, Zn). Our results offer additional insights on DDE characterization and pathogenesis, highlight the potentiality of colorimetric measurements in their clinical diagnosis and provide leads to improve the performance of minimally invasive restorative strategies.

Keywords: Developmental Defect of Enamel, crystallography, Electron Microscopy, Nuclear Techniques, Atom Probe Tomography.

1. Introduction

Amelogenesis begins in the third trimester of fetal life and continues until six years after birth [1]. This process follows a well-characterized spatiotemporal sequence driven by the differentiation and function of ameloblast cells [2]. During the secretory stage, the enamel matrix is deposited. Mineral ribbons are formed running from the dentin enamel junction (DEJ) towards the enamel surface. Subsequently, matrix proteins are proteolyzed and removed, leaving enough space for apatite crystallites to thicken until a final enamel mineral density of approximately 96% is reached. After tooth eruption, enamel is bolstered due to its contact with the ion-rich oral environnement participating in repair of minimal reversible demineralization that normally occurs in the buccal environment. However, as ameloblasts are lost during tooth eruption, developmental defects of enamel (DDE) are irreversible, thus requiring reparative treatments [3]. Environmental stressors during enamel formation generate two main types of defects: enamel hypoplasia and hypomineralization. Enamel hypoplasia is a defect that affects enamel thickness. By contrast, enamel hypomineralization is characterized by an increase in porosity with an otherwise normal volume, until enamel breaks down in the most severe forms. Hypomineralization occurs in the context of dental fluorosis (DF) due to excessive absorption of fluoride (F) [4], and in molar incisor hypomineralization (MIH), for which the etiology is still unclear [5]. DF affects more than 250 millions people worldwide [6] and MIH impacts 14-15% of 6-9 year old children [7] [8]. However, the clinical presentations of these conditions are extremely variable, and their differential diagnosis can be challenging. Finally, best practices for clinical management of hypomineralized teeth, including pain management, placement and longevity of restorations, and aesthetic issues remain an area of active research [9] [10].

DF results from systemic fluoride exposure during tooth formation in late pregnancy and infancy [11] [12]. The mildest form of DF causes loss of the tooth’s natural shiny appearance and

the development of chalky, white spots. With increasing severity, these qualitative colour abnormalities vary from yellow to brown and to (rarely) black. In the most severe cases, enamel can even be lost, causing the tooth to be pitted or corroded. The mechanism of fluoride toxicity involves several events in both intracellular and extracellular compartments [13]. In the extracellular compartment, F^- interacts with the forming mineral and inhibits proteolytic enzymes [14]. In ameloblasts, F^- affects expression of a limited number of key genes in the mineralization process, such as those encoding matrix protein amelogenin [15] and proteolytic enzymes KLK-4 and MMP-20 [16]. Excessive F^- exposure in rodent incisors also alters iron metabolism, resulting in a disordered distribution of Fe in enamel [17]. Importantly, emerging literature raises the question of environmental pollutants as contributors to DF. In particular, it was found that co-exposure to F^- and Bisphenol A worsens DF in rodents [18]. Similarly, clinical studies suggest that even low doses of fluoride may be associated with increased risk of DF [19]. These experimental and clinical data raise additional questions regarding the mechanism by which F^- affects enamel, and how it acts in pathogenic synergy with other factors present in the human environment [20] [18].

Compared to DF, MIH development and causes are less clear [21, 22]. Environmental factors such as endocrine disruptors, including dioxin [23] or bisphenol A [24], antibiotics or/and early childhood diseases, and vitamin D deficiency are potential causal factors. Similarly to DF, early signs of MIH include the development of chalky white spots (or lesions) on permanent first molars and occasionally incisors. These lesions worsen from yellow to brown with increasing severity of MIH. In these colored lesions, an overabundance of albumin has been suggested to act as a direct inhibitor of enamel crystal growth [24] [25] [26]. Increased enamelin expression associated with a decrease in KLK-4 expression by ameloblast was observed [24]. In addition, the presence of greater amounts of phospholipids indicates that MIH enamel did not achieve its complete maturation [27].

Altogether, many questions and challenges remain to improve our understanding of DDE. In this study, we hypothesized that a systematic comparison of the composition and structure of enamel

impacted by MIH and DF would not only offer additional insights on their etiology but also pave the way for improved diagnostics, preventive measures, and therapeutic strategies, including restorative biomaterials [28] [29]. With this aim, we drew on a wide range of characterization techniques allowing comparison of optical, chemical, structural and mechanical properties of heathy and DDE-affected enamel from the macro- to the nano-scale. Structural analysis was first performed at the micro- and nanoscale using Scaning- (SEM), Transmission- (TEM) and Scanning Transmission Electron Microscopy (STEM) [30], and explored crystallite organization using Atom Probe Tomography (APT) [31] which has so far never been applied to DDE. X-Ray Diffraction (XRD) allows nanoscale structural investigations. Combined with Attenuated Total Reflectance-Fourier Transformed Infra-Red (ATR-FITR), these techniques also delivered information on enamel chemical properties with location of trace elements, ions and organic material. These data were complemented with those obtained with particle-induced X-ray and gamma-ray emission (PIXE/PIGE) that allows semi-quantifications of trace elements and ions in enamel surface [32] and Inductively Coupled Plasma (ICP) spectrometry (ICP-MS and ICP-OES) for trace elements analysis in whole lesion. Finally, a procedure for refining color analysis measurements, a current clinical tool [33], has been established and applied here to *in situ* DDE samples, including 120 teeth with MIH and 94 teeth with DF. Our data highlight that DDE mainly impact enamel structure and composition at the microscale while variations evidenced at the nanoscale were small and mostly related to lesion severity. However, the combination of changes at multiple scales translates into distinct colorimetric parameters, making their measurement a method of choice for a more sensitive and specific clinical diagnosis of DDE.

2. Material and Methods

2.1 Study Approval

All patients (or parents in the case of minor participants) gave their written informed consent prior to participation. Patients gave a separate written informed consent for the use of the photographs. Subjects' rights were protected by an appropriate Institutional Review Board. Authorization agreements from the Patient Protection Committee have been obtained for the performance of this clinical study (ID-RCB:2019-A00052-55, file N°: 19.02.18.62108) recorded with the following trial: ClinicalTrials.gov NCT04704089.

2.2 Patient recruitment and dental enamel samples selection and collection

Thirty-two patients with mild or severe dental fluorosis (DF), 42 patients with mild or severe MIH and 15 patients with Healthy Enamel (HE) were involved in the study. All patients (57 % men and 43 % women) were between 9 and 25 years of age and recruited either from the Centres de Reference/de Compétence des maladies dentaires et orales rares (O-Rares) at Hôpital Rothschild and Hôpital La Pitié-Salpêtrière respectively. Inclusion and exclusion criteria were based on those established by the international consensus on MIH and DF diagnosis [34]. Positive diagnosis was based on the clinical singularity of DDE: random demarcated for MIH or diffuse opacities or patches for DF, tooth-type selectivity. Differential diagnosis with hypomature amelogenesis imperfecta and punctual inflammation-induced hypomineralization of permanent teeth was established by their distinct clinical features and familial and medical antecedent analysis. The severity of each lesion, graded clinically as mild or severe forms (following the guidelines from European Archives of Pediatric Dentistry, EAPD [35]) was used in this study. The mild forms exhibited opaque white color lesions and severe forms were colored in yellow to brown. Human dental enamel samples were collected either as a whole tooth, when the extraction was indicated for periodontal reasons (incisors or molars), or as lesional region after selective drilling on the patient's tooth (incisors or molars) with the use of a diamond micro-saw (Komet® ref. 6911H.104/943CH.204;080). Selective drilling was always performed at the center of the lesion.

Detailed sample selection and a summary of the number and the distribution of samples for each technique are shown in detail in Table 1. The collected samples were cleaned 3 times in 70% ethanol and stored at - 80°C. The samples were then either directly proceeded or included in the epoxy resin or reduced to powder depending on the techniques used for investigations. Each sample was dedicated to specific type of analyses without prior selection.

Techniques	Developmental Defect of Enamel				Healthy Enamel
	MIH		DF		
	Mild	Severe	Mild	Severe	
Spectrophotometry	42 patients 120 teeth 45 ua		32 patients 94 teeth -		15 patients 21 teeth -
SEM	M1 M2	M6 M7	M8 M9	M11 M12	PM1 PM2
STEM & HR-TEM	M3	M6	M10	M11 M12	- -
Nanoindentation	M5		I9 I10	I14 M13	I16 -
XRD	M4 I3 I4	M7 I5 I6	I11 I12 M8	I15 M14 -	M17 PM2 ua M1
FTIR	M3 I1 I2	M6 I3 I4	M10 I13	M11 M15 M16	PM1 ua M2 ua M3
PIGE-PIXE	M3 I1 I2	M6 I7 I8	M10 I13	M11 M12 M13	PM1 ua M2 ua M3
ICP-MS/OES	M4 I3 I4	M7 I5 I6	I11 I12 M10	I15 M14 -	M17 PM2 uaM1
APT	M1 (4 tips) M2 (4 tips)	M6 (4 tips) M7 (4 tips)	M8 (2 tips) M9 (3 tips)	M11 (4 tips) M12 (4 tips)	*De Rocher et al.2020*

Table 1: Overview of the samples used in this study for each technique. ua = unaffected area, M = molar, PM = premolar, I = incisor.

2.3 Color Analysis

Color analysis was built up from the color data captured with a spectrophotometer model (SpectroShade Micro®, MHT) based on CIE *L*a*b** color space coordinates. L: lightness, a: chroma along red-green axis and b: chroma along yellow-blue axis [36]. All SpectroShade assessments were performed by one trained operator (S. Houari). To obtain the *L*a*b** values used

for this study, healthy enamel (HE) from control patients and manual delimitations of unaffected enamel and lesional enamel (mild and severe forms of DF and MIH) from patients presenting one of these DDE were taken from the spectroshade images (Table S 1 and Figure S 1). Their values in the CIELab color space were then averaged. For comparison, *L*a*b** values obtained directly from the spectrophotometer, using standard geometric shapes, were presented in Table S 2. The software used for image analysis has been developed within a collaboration with Dental Monitoring® company using the Python [37] (version 3.7.3) package OpenCV (version 4.1.2.30). Detailed notes on color space conversion were reported in the Open Source Computer Vision [38].

2.4 Nanoindentation

Nanoindentation was performed on sagittal sections of human incisors and molars using a calibrated Berkovich nanoindenter (XP, MTS with Continuous Stiffness Measurement (CSM) module). Detailed informations are provided in Supplementary Material.

2.5 Scanning Electron Microscopy (SEM)

Human enamel slice surfaces were etched with 250 mM nitric acid adjusted to pH = 4 for 30 to 45 s, to reveal rod and inter-rod microstructure. Each sample was coated with a 8 nm thick layer of platinum (Pt) in a vacuum evaporator, and the enamel microstructure was observed with HR-SEM microscope (Carl Zeiss Supra 40; Carl Zeiss AG, Oberkochen, Germany) at 10 kV. All images were taken from outer surface of enamel (200 first µm). Detailed informations are provided in Supplementary Material.

2.6 Transmission Electron Microscopy (TEM)

All TEM-analysed samples were prepared in cross-sectional orientation, going from the surface towards the inside of the tooth. For preparation of TEM samples from specific areas, the focused ion beam (FIB) technique was applied using FEI Scios DualBeam system (Thermo Fischer Scientific, Inc.) with a Ga^+ ion beam source. Samples were first coated with 10 nm thick carbon layer by thermal evaporation (Leica EM ACE 600 coater system) and the area of interest further coated with a Pt layer. The FIB was operated at 30 kV beam energy. Coarse milling was performed using

a beam current of 5 and 3 nA. Afterward, the samples were lifted-out using an in-situ micromanipulator and fastened to a half-moon-shaped copper (Cu) ring using Pt. FIB lamellae were milled from both sides at an accelerating voltage of 16 kV and beam current 0.25 nA. Several smaller regions were further milled at an accelerating voltage of 8 kV using a beam current of 25 pA, which was then reduced to 5 kV at the beam current of 16 pA. Finally, samples were cleaned at an accelerating voltage of 2 kV and beam current of 8.9 pA. High-resolution transmission electron microscopy (HRTEM) observations were carried out at 80 kV with an advanced TEM (JEOL ARM200F, JEOL Co. Ltd.), equipped with a cold field-emission gun and a CETCOR image corrector (CEOS Co. Ltd.). Bright field (BF-) and high-angle annular dark-field (HAADF-) scanning TEM (STEM) imaging combined with energy-dispersive X-ray spectroscopy (EDX) measurements were carried out at 60 kV with an advanced analytical TEM/STEM (JEOL ARM200F, JEOL Co. Ltd.), equipped with a cold field emission gun and a DCOR probe Cs-corrector (CEOS Co. Ltd.).

2.7 Particle-Induced X-ray Emission (PIXE) and Gamma-ray Emission (PIGE)

The Mini-Beam Setup installed on one beam line of the CEMHTI Pelletron was equipped with a five positions sample-holder which can be moved by X and Y translation motors an endoscope allowed to visualize the beam on a 500 x 500 μm^2 window of the sample surface. An X-ray detector (SDD Silicon Drift detector) and a gamma-ray detector (HPGe High Purity Germanium) were installed on the Mini-Beam Setup to realize the coupling of PIXE et PIGE techniques. The ionic optics on this beam line was optimized to obtain a lateral resolution around 30-50 µm. Outer surface of lesioned or unaffected enamel were analyzed as an area of 200 x 200 μm^2 with a proton beam of 2.8 MeV energy. The analysis depth was 50 µm. The standards used for the quantification of F, Na, Mg and P were CaF_2, NaF, Mg and synthetic hydroxyapatite. The Zn and Fe mass concentrations were quantified by PIXE using two standards (Pure Zn metal and BCR SRM 110 international standard at Zn concentration of 52.1 % and Fe of 0.55 %).

2.8 Inductively Coupled Plasma Mass Spectrometry (ICP-MS) and Inductively Coupled Plasma Optical Emission Spectrometry (ICP-OES)

Quantification of trace elements was accomplished using ICP-MS and ICP-OES of acid digested samples (n= 2/condition of severity). Specifically, the sample was digested in concentrated nitric acid (> 69%) (Thermo Fisher Scientific, Waltham, MA, USA) at 65°C for at least 3 hours. Each sample was acquired by 3 main (peak jumping) runs (40 sweeps). The isotopes selected for analysis were ^{56}Fe, ^{57}Fe, ^{64}Zn, ^{66}Zn, ^{68}Zn, ^{88}Sr, and ^{89}Y, ^{115}In, ^{159}Tb, (chosen as internal standards for data interpolation and machine stability). ICP-OES was performed on a computer-controlled (QTEGRA software) Thermo iCap7600. ICP-OES (Thermo Fisher Scientific, Waltham, MA, USA) operating in radial view and equipped with a CETAC 520 autosampler (Omaha, NE, USA). Each sample was acquired using 5 second visible exposure time and 15 second UV exposure time, running 3 replicates. The spectral lines selected for analysis were: Na (588.995, 589.592, 818.326 nm), Mg (279.553, 280.270, 285.213 nm) K (766.490, 404.414, 769.896 nm), Ca (393.366, 396.847, 422.673), P (177.495, 178.284, 213.618 nm), and S (180.731, 182.034, 182.624 nm).

2.9 Attenuated Total Reflectance-Fourier Transformed Infra-Red (ATR-FTIR)

ATR-FTIR spectra were recorded on powdered enamel samples using a Quest ATR device and a Nicolet 6700 FTIR spectrometer. Spectra were recorded between 400 and 4000 cm^{-1} by averaging 100 scans with a resolution of 1 cm^{-1}.

2.10 X-Ray diffraction (XRD)

A Bruker Molly instrument which runs on a MoKα (λ = 0.71073 Å) micro-source with a beam size of ~ 120 µm diameter was used to measure the small enamel samples (2 mm ∅) in transmission geometry. Bulk millimeter-size enamel samples were fixed on a nylon loop using paratone oil. Two-dimensional X-ray diffraction data in transmission geometry were collected at room temperature for each sample (n = 2 enamel samples/condition of severity). Detector distance was set at 15 cm. Data was collected using multiple detector positions in order to cover a wide range of diffraction angles. The exposure time was 300 s. Data were merged across the angular range

and integrated over an azimuthal wedge of 10˚ using the Bruker Diffract.EVA software. The azimuthal position (e.g., 45°, 135°, 210° and 300°) provided in the supporting information section refers to the center of the integration wedge, e.g., the 45° section corresponds to the integrated area between the gamma limits from 40° to 50°. Diffractometer and beam center were calibrated using an Ylid standard crystal provided by Bruker. Background subtraction was performed by fitting a second order polynomial within Diffract.EVA.

2.11 Atom Probe Tomography (APT)

Samples were embedded in Epo-Tek 301 epoxy and sectioned, so the region of interest (i.e., lesion) was exposed. Surfaces were ground and polished as described above, rinsed in DI water and dried in air. Unless otherwise noted, samples were affixed to an aluminum stub using carbon tape and coated with AuPd (~25 nm) using a Denton Desk IV sputter coating system (Denton Vacuum, Moorestown, NJ). The surface of the sample was then grounded to the stub using colloidal silver paint. A Dual Beam SEM/FIB (Helios NanoLab; FEI Company) was used to extract two 30 µm x 2 µm liftouts from MIH and DF lesions in two separate patients exhibiting each pathology. From these liftouts, a total of 16 tips for MIH and 13 tips for DF, from a total of 4 different patients, were prepared. APT analysis was performed using a LEAP 5000 XS (CAMECA Instruments) with a laser operating at a wavelength of 355 nm, a power of 40 pJ, and a pulse frequency of 250 kHz. In the analysis chamber, the temperature was set to 25 K and the vacuum was maintained at $<10^{-8}$ Pa (Table S 3). The DC potential on the microtip was adjusted to maintain an evaporation rate of 0.005 ions per laser pulse. 3D reconstructions of the sample tips were made using the IVAS software package (CAMECA Instruments). Standard parameters were used for all reconstructions. Data previously obtained on HE [31] were used for comparison. 1D concentration profiles showing the distribution of ions were generated by isolating a cylindrical region of interest (ROI) across enamel crystallites visible in the 3D reconstruction.

2.12 Statistics

All data were expressed as the mean ± standard deviation (SD). Kruskal-Wallis followed by Dunn's multiple comparisons test was used for statistical analysis. All calculations were carried out using GraphPad Prism Software Version 9.0 (GraphPad Software Inc., La Jolla, CA). If $p<0.05$(*), $p<0.01$(**) or $p<0.001$(***), the values compared were considered to be significantly different. Multiple comparisons of trace element concentrations (in at%) was performed on the data from APT experiments.

3. Results

3.1 Color parameters

Color parameters were defined as the lightness (L^*), the level (saturation) of green-red (a^*) and the level yellow-blue (b^*). Colors of DDE (Figure 1A) were analyzed using a spectrophotometer in the CIELab space directly on patients' teeth representing 120 teeth with MIH, 94 with DF and 21 teeth from healthy patients without any diagnosed DDE (Table 1). Measured color parameters in all lesions formed a cluster, ranging from bright to dark with low saturated colors, passing through more saturated shades, especially along the b^* axis (Figure 1B). Starting from the highest values of L^* with low values of a^* and b^*, the first region corresponded enamel affected by mild fluorosis. The centroid of this region was located at the coordinates (67, 5.8, 9.1) (Table S 1 and Table S 2). Following the cluster from top to bottom, with slightly lower values of L^* and higher values of a^* and b^* especially, was found the group of mild MIH, corresponding to white spots, whose centroid was (60.8, 6.9, 16.7). The group in the middle was healthy control teeth (black) located around (63.7, 9.1, 20.7) which was different from the unaffected areas from MIH patients (grey) located around (58.4, 12.8, 24). Slightly less compact was the group of severe MIH, corresponding to brown spots, located around (51,18.7,31.9) with lower brightness and higher saturation than HE. The severe fluorosis or brown spots were the darkest of all and were located around (24, 22.6, 24.3) with a much lower L^* values than all other groups (Table S 2). Overall MIH lesions

formed the most heterogeneous group with some values overlapping with the healthy group but severe MIH were discriminated with a much higher *b** values than all other groups.

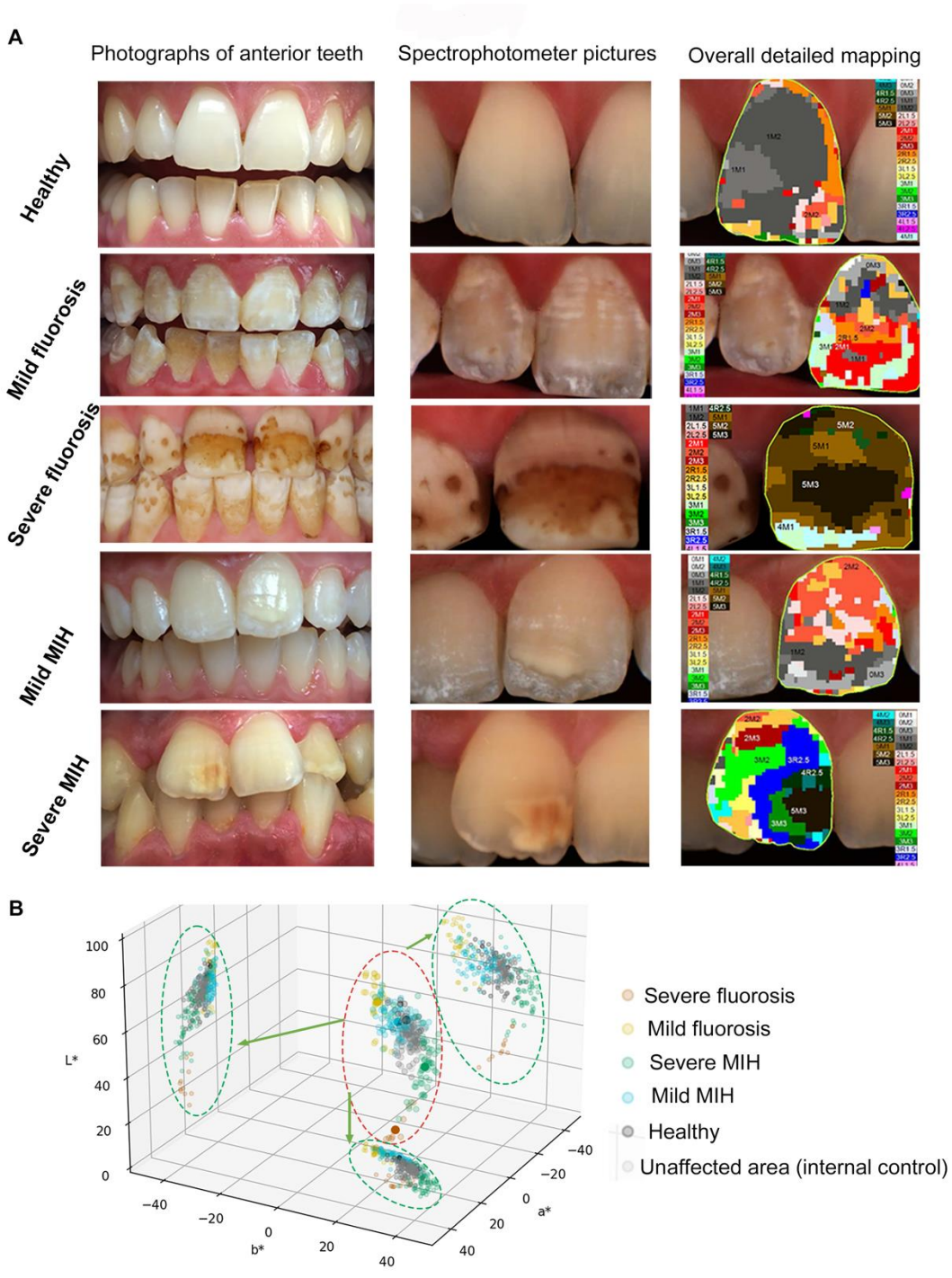

Figure 1 : DDE digital tooth color measurements. A Photographs of anterior teeth representative of each pathology according to the severity classification compared to healthy ones from control patients. Spectrophotometer pictures of representative teeth. Detailed color maps provided by the Spectroshade MHT® based on the analog VITA 3D MASTER shade guide. **B** Point cloud representation of *L*a*b** coordinates

in CIELab color space of each of the teeth analysed. The main 3D representation is surrounded by a red ellipse. Each small dot represents the average color coordinates for a selected area on a tooth and each bigger dot represents the centroid of one analysis condition. Projections onto the L*a*, L*b*, and a*b* planes (green ellipses) are additionally drawn to better visualize the distributions.

3.2 Mechanical properties and nanostructure

Representative samples used for nanoindentation experiments are shown in Figure S 2. DF resulted in an constant slight reduction of hardness (0.5-0.7 GPa) in the inner and the middle layer of enamel, and up to 1 GPa in the outer layer (Figure 2A). Contrary to HE, hardness of DF decreased in outer layer (Figure 2A). MIH reduced the hardness of enamel by 2 GPa for mild lesions and by 3 GPa for severe lesions (Figure 2B). Severe lesions affected mainly inner and middle layers of enamel. Optical images presented in Figure S 2D and 2E show that MIH lesion started in the inner layer of enamel, close to the dentin-enamel junction and, depending on the severity, extended up to the surface of the enamel. Due to the location of severe MIH lesions analyzed on the occlusal side, they exhibited higher hardness on the last 300 µm of the outer layer of enamel compared to mild lesions located on the lingual side where unaffected enamel had lower hardness values (Figure 2B).

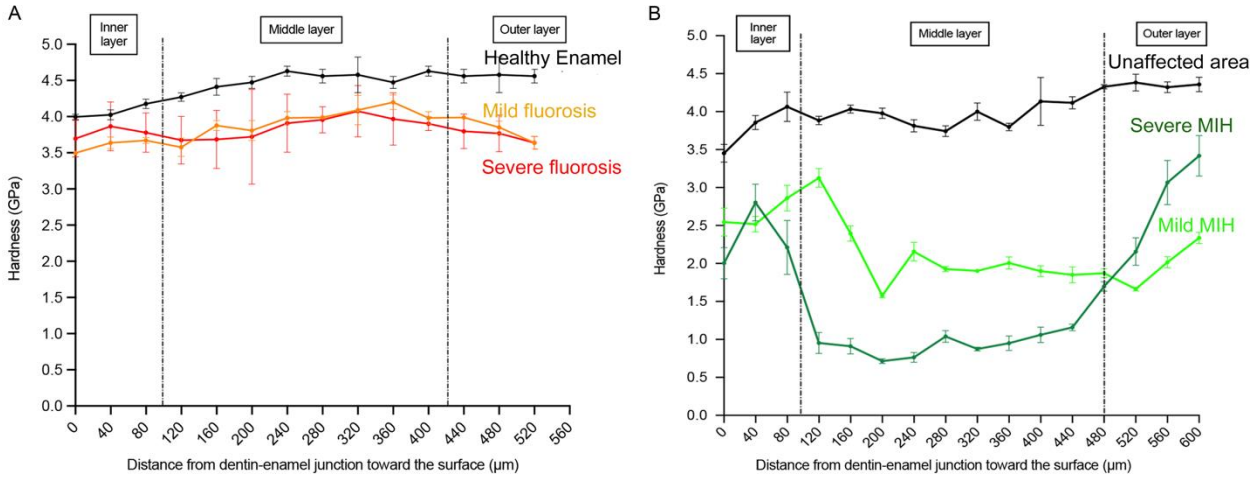

Figure 2: DDE mechanical properties. A Enamel hardness as a function of distance from the dentin-enamel junction (DEJ) to the surface (µm), comparing healthy enamel (HE) (control patients) with enamel from patients with mild and severe fluorosis. **B** Enamel Hardness as a function of distance from the DEJ to the enamel external surface, comparing unaffected areas**,** mild and severe MIH lesions. Inner (first 100 µm), middle, and outer enamel (last 100 µm) layers are delimitated by dashed lines.

All zones of interest (red circles or boxes, Figure 3A) observed by SEM were located in the outer 1/3 of enamel. In severe DDE lesions, the rod sheath surrounding enamel rods, was more clearly observed compared to the HE and mild DDE forms. When compared to HE, all DF lesions exhibited porosities in which the crystallites were wide and rough and the interrod gaps widened. Severe DF lesions exhibited some additional amorphous-like material (black arrows, Figure 3B). MIH lesions contained less distinct enamel rods often covered by a structureless layer and containing small and thin crystallites without clear difference between mild and severe forms (Figure 3B). Following in vitro acid etching, crystallites exhibited a hollow structure (Figure 3C). Crystallite cores appeared thinner in MIH than in HE and more homogeneous and more elongated in DF than in other conditions (Figure 3C).

HR-TEM and STEM analyses combined with EDX were performed on severe DF samples that showed a characteristic striated pattern pathognomonic of DF, with interchanging dark and light bands (Figure 3D and Figure S 3 for enlarged images). At the nanometer scale, only dark areas were severely affected, resulting in a surface layer consisting of “shattered” disordered hydroxyapatite crystals (SA) that extended down to approximately 300 nm inside the tooth. Underneath, elongated HA crystals were forming dense enamel. EDX measurements showed a significantly higher level of F in the dark shattered areas than in “normal” enamel underneath, that decreased with depth. In parallel, a slight decrease in the Ca/P ratio and increase in sodium (Na) content with depth was measured but the differences between SA and HA were not significant. In contrast, STEM/EDX analyses performed on enamel surface of mild DF and MIH samples did not reveal detectable changes in chemistry but demineralized and rough crystallites on the surface of MIH samples (Figure S 4).

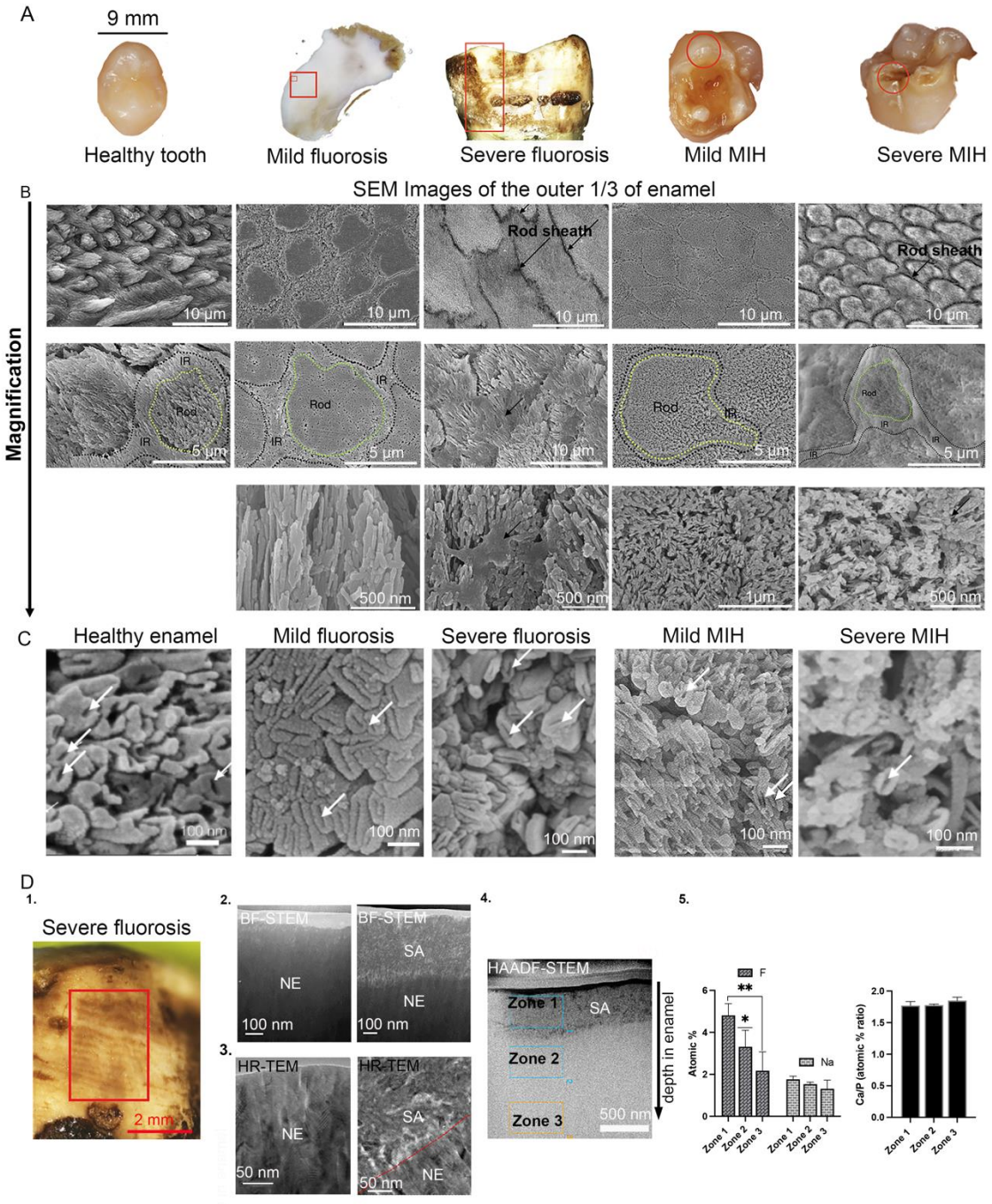

Figure 3: DDE ultrastructure by Electron Microscopy. A Representative images of each condition. **B** SEM images of sections through the outer layer of enamel lesions compared to the healthy enamel. Rod and interrod (IR) enamel are indicated by dotted green and black lines respectively. **C** SEM images of sections showing enamel crystallites in healthy enamel (33) and enamel lesions. White arrows indicate where preferential dissolution of the crystallite core resulted in formation of hollow crystallites. Scale bar: 100 nm. **D 1.** Macroscopic view of surface enamel from a tooth with severe DF. Scale bar: 2 mm. **2.** BF-STEM images from light band (left) showing "normal" enamel (NE) and a dark band (right) showing a "shattered area" (SA) underneath followed by NE. Scale bar: 100 nm. **3.** HR-TEM images from light band (left) and dark band (right). Scale bar: 50 nm. **4.** HAADF-STEM image visualizing from the surface to ≅ 2 µm deep into the enamel. Scale bar: 500 nm. **5.** Bar plot of mean atomic fractions of F and Na, and of the ratio of the atomic fractions of calcium over that of phosphorous (Ca/P) for each zone, as assessed using STEM-EDX. Zone 1 corresponds to the SA. n = 6 measurements/zone on 2 different teeth.

3.3 Crystalline structure

Microdiffraction experiments showed different structural organizations in HE and mild and severe DF or MIH, based on 2D and radially integrated diffraction patterns (Figure S 5). Diffraction patterns of enamel from all conditions showed Bragg peaks related to crystalline apatite and an additional broad band with a maximum around $2\theta \cong$ 5°-10°. However, the intensity and width of the peaks varied with the considered pathology and severity (Figure 4A). For DF, the signal was always dominated by the Bragg peaks although a small fraction of amorphous phase was detectable in the severe cases (Figure 4A). An increase in the full width at half maximum (FWHM) of some of the peaks was noticed. In contrast, for MIH, the FWHM did not seem modified but the broad signal was more intense especially in the severe case.

Selected diffraction analysis on a section of a tooth exhibiting severe DF showed no variation of the crystallography between affected region (1), transitional region (2) and unaffected region (3) (Figure 4B). Importantly, the angular dependence of the micro-XRD patterns was similar for the three measurements indicating that healthy and lesional enamel displayed similar crystal orientation distribution at the micron scale.

3.4 ATR-FTIR analysis

The ATR-FTIR spectra of the control (HE), DF and MIH enamel samples presented the characteristic absorption bands ascribed to the internal vibrations of the phosphate groups and structural carbonate incorporated at the A and B sites (hydroxyl and phosphate sites, respectively) of the apatite structure (Figure 4C). The intense band observed between 990 and 1100 cm^{-1} corresponds to the $\nu_3(PO_4)$ stretching mode of the structural phosphate group while the weaker band at 960 cm^{-1} corresponds to the $\nu_1(PO_4)$ stretching mode. The position of the $\nu_1(PO_4)$ phosphate band remained between 959.9 and 958.9 cm^{-1} for all samples, a range consistent with values found for biogenic apatites. The observation of the OH bending mode at 630 cm^{-1} in all samples,

including the DF ones, confirmed the presence of hydroxyl groups in the channel sites, indicating a low rate of F^- substitution. Regarding the structural carbonate groups, the $\nu_2(CO_3)$ band displayed the two characteristic bands associated with A-type and B-type carbonate substitutions (Figure 4C). The signal corresponding to a clumped (F^-, CO_3^{2-}) defect (reported in artificially fluorinated bones) was not observed at 863 cm^{-1}. Additional examination of the $\nu_3(CO_3)$ bands (Figure 4C) revealed no significant variation of the A-type to B-type carbonate ratio throughout the sample series. Among all samples, the most different spectrum was severe MIH (Figure 4C), which displayed well-identified amide bands (I, II and III) at 1660, 1540 and 1250 cm^{-1} respectively (Figure 4C). These characteristic bands suggested the occurrence of a significant protein fraction in severe MIH samples. Additionally, the broad band at 1640 cm^{-1} corresponding to the bending mode of associated water molecules was observed in all samples.

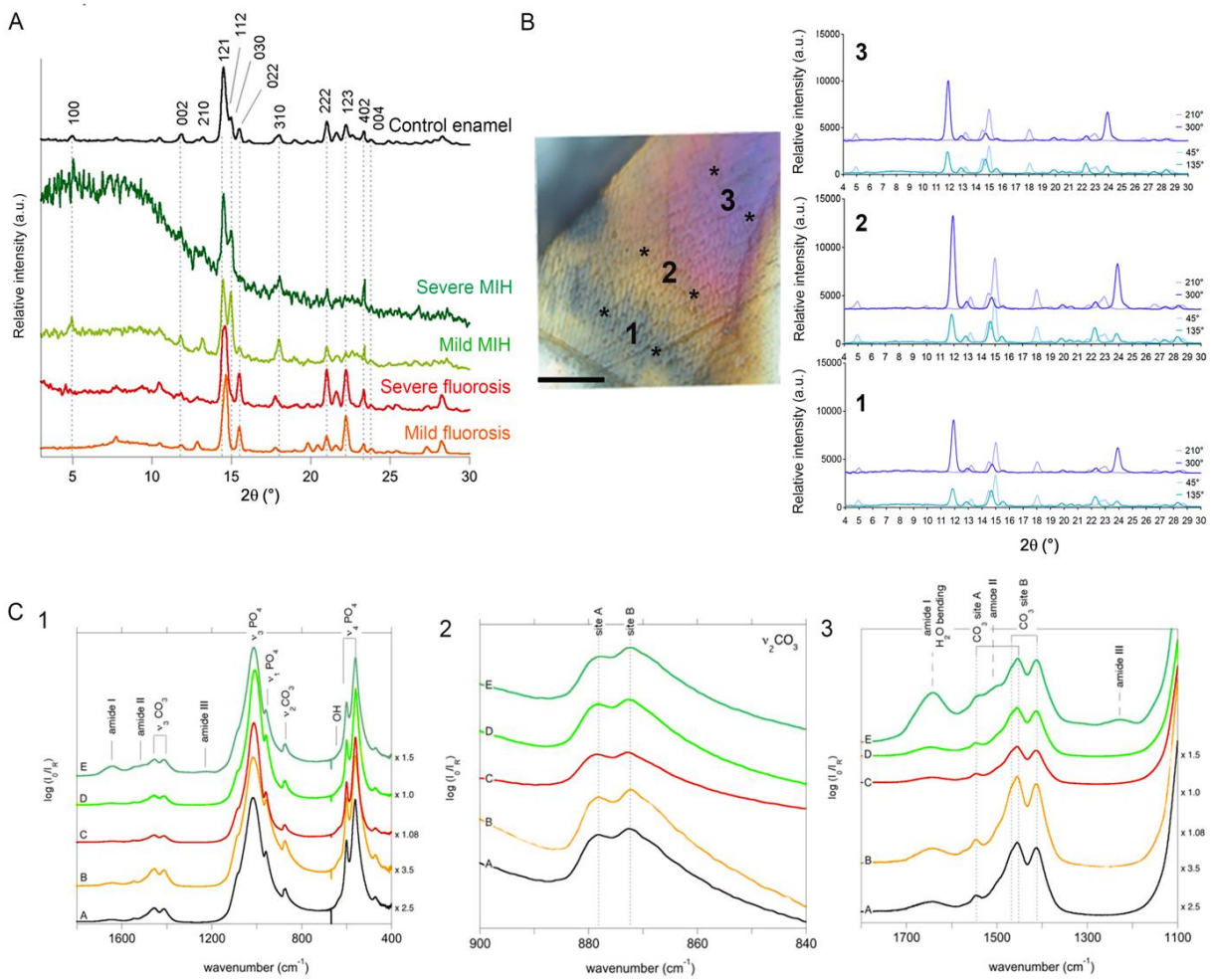

Figure 4: Crystallographic and spectroscopic characterizations of DDE. A X-ray diffraction patternsof each condition. Miller indices for hydroxyapatite reflections are provided above the sample labeled 'control enamel' (black line). The diffractograms have been normalized to the intensity of the most intense Bragg peak and have been vertically shifted by an arbitrary value to allow their comparison. n=2 enamel samples/condition of severity. **B** Optical image of a severe DF sample used for the 2D diffraction experiment (scale bar: 100 µm) containing an affected region (1), a transitional region (2) and an unaffected region (3). Diffraction data on 2 different points for each region (marked with a star *) were collected and averaged. One-dimensional diffraction patterns after integrating the 2D diffraction data. **C1** ATR-FTIR spectra of Healthy Enamel (HE) (black line A) compared to mild DF (orange line B), severe DF (red line C), mild MIH (light green line D) and severe MIH (dark green line E). **C2** Region of the ATR-FTIR spectra showing the v_2CO_3 bands. **C3** Region of the ATR-FTIR spectra showing the v_3CO_3 bands. Spectra were multiplied by an arbitrary scale factor (indicated on the right) and shifted vertically to facilitate their comparison.

3.5 Elemental composition and spatial distribution

PIGE was used to determine the mass fraction of Na, P, F and Mg with a 200 µm lateral resolution and a probed depth of 50 µm from the outer surface of enamel. Some representative spectra are provided in Figure S 6 and resulting data are gathered in Figure 5A. As expected, F amounts

were statistically the highest in severe DF (approximately 4000 ppm compared to 350 ppm in mild DF and 200 ppm in HE) (Figure 5A). Interestingly, the outer surface of MIH enamel also contained a high amount of F whose value ranges between mild and severe DF. Na concentrations measured by PIGE technique were significantly lower in mild and severe MIH. P concentrations did not vary whatever the pathology compared to the HE. Mg levels were below the detection limit (6000 ppm). ICP-OES analysis of whole lesion showed no significant variations in Ca, Na, P and Mg contents between the different samples (Figure 5B).

PIXE and ICP-MS were used to quantify Fe and Zn content on the outer surface and within whole lesion, respectively (Figure 5C, 5D and Figure S 6). Compared to HE, Zn levels were significantly increased only in the outer surface of both MIH defects and in the bulk of mild MIH. Higher levels of Fe compared to HE were detected in all DDE, both on the outer surface and in bulk, except for mild DF (Figure 5C).

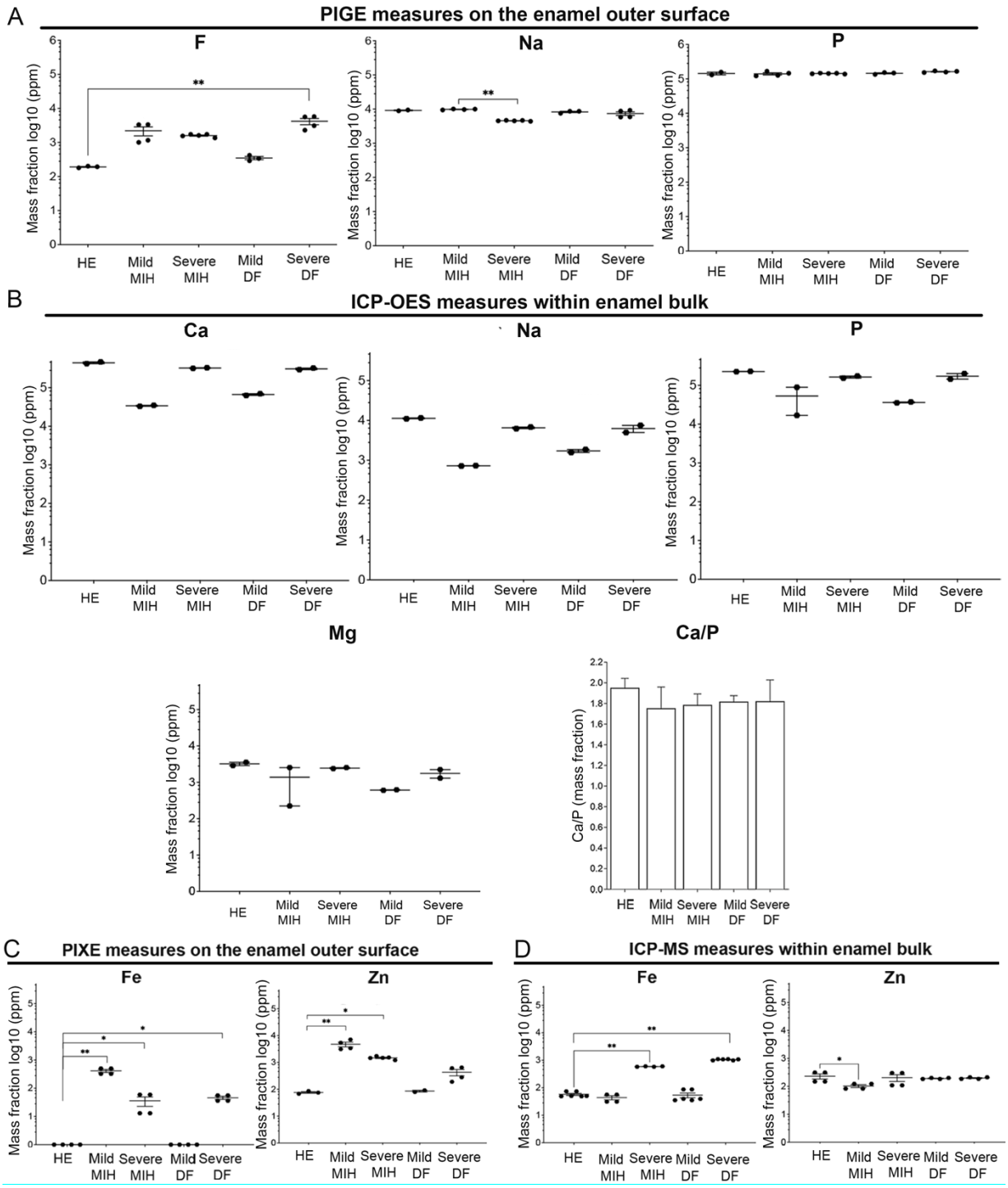

Figure 5: DDE chemical composition. A Plot of mass fraction of F, Na and P on the outer surface of enamel, as assessed by PIGE. n= 2 to 4 measurement points on 2 different samples/condition. **B** Plot of mass fraction of Ca, Na, P and Mg in the lesion body, using ICP-OES. Ca/P ratios were calculated from mass fractions. n= 2 samples/condition. **C** Mass fraction of trace elements Fe and Zn measured on the outer surface of enamel by PIXE. n= 4 measurement points on 2 different samples/condition. **D** Mass fraction of trace elements Fe and Zn measured in the body of the lesion by ICP-MS. n= 2 samples/condition. Note that for all plots but for the Ca/P ratio, the decadic logarithm of the mass fraction (in ppm) is given.

APT allowed to analyze the spatial distribution of Mg^{2+}, Na^{+}, F^{-} and COH/carbon at the nanoscale (Figure 6). 3D reconstructions of sample tips (Figure 6) highlighted that fundamental aspects of the structure of healthy enamel were preserved in all samples. Specifically, crystallite cross sections were predominantly convex polygons with an edge length of 20-50 nm in the short and 70-170 nm in the long direction. Crystallites exhibited a core (co) - shell (sh) architecture and were separated by a thin intergranular layer (ig). In all samples, F, Mg and Na contents were higher in the core compared to the shell, whereas C content was comparable. In all crystallite parts, Na was higher in severe DDE, especially MIH. In external layers (sh and ig), F was higher in DF than in MIH. Noticeably, Fe was detected in severe DF samples (Figure S 7).

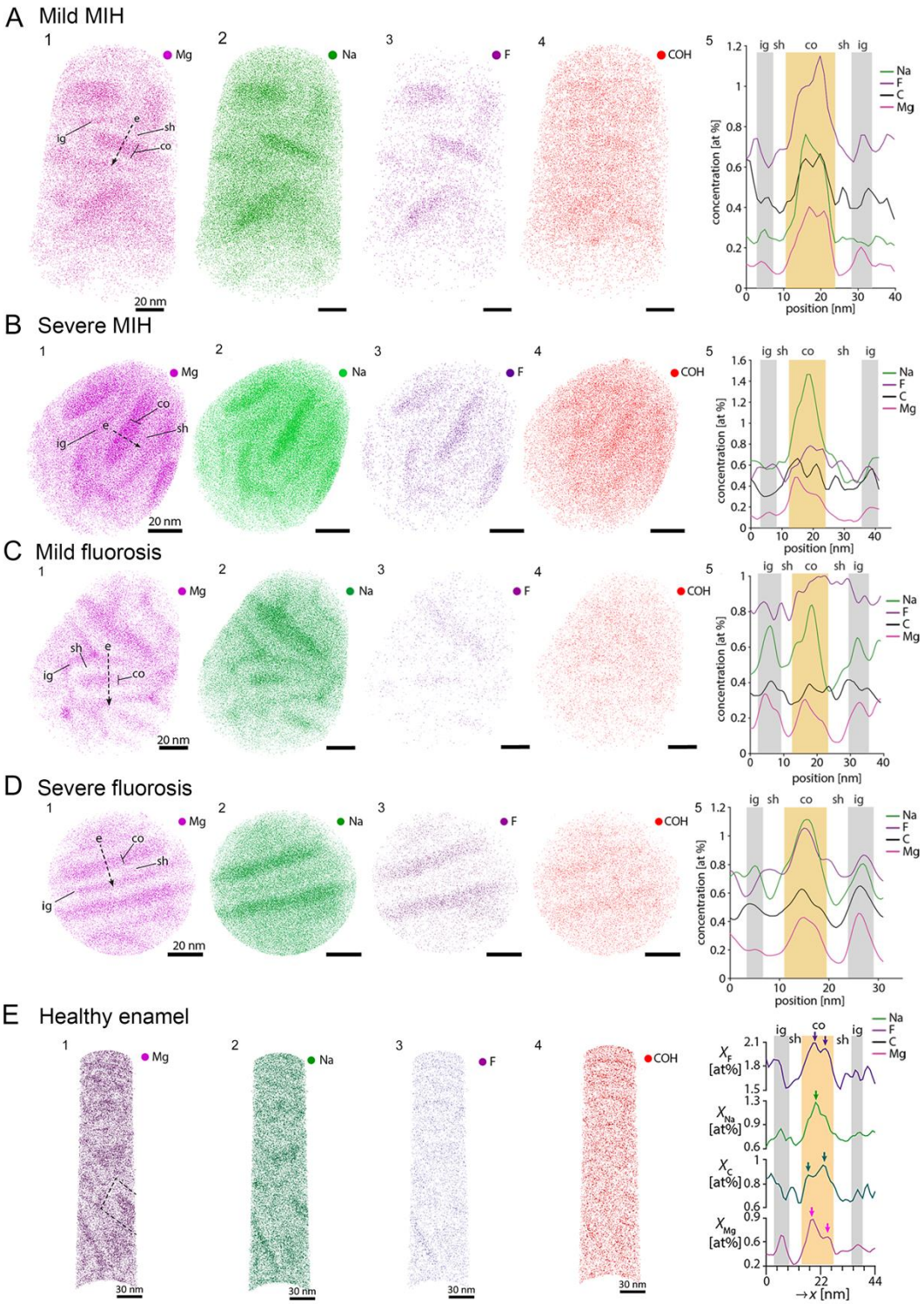

Figure 6: Atomic-scale DDE structure and composition. APT 3D reconstructions of (**A)** mild MIH enamel, (**B**) severe MIH enamel, (**C**) mild DF enamel, (**D**) severe DF enamel, and (**E**) healthy enamel for comparison (33) with intergranular (ig), shell (sh) and core (co) regions of crystallites indicated. **1.** Mg distribution. **2.** Na distribution. **3.** F distribution. **4.** Carbonyl (COH) distribution, **5.** 1D concentration profile elucidates the distribution of ions across a crystallite. Scale bars: (A – D) 20 nm, (E) 30 nm. n= 16 tips for MIH from 2 patients and 13 tips for DF from 2 patients.

4. Discussion

4.1 Multi-scale characterization of DDE

The main aim of this work was to improve the current understanding of the impact of DDE on enamel structure and composition. In DF lesions, enamel microstructure as observed using SEM and STEM / HR-TEM is characterized by wide and rough crystallites with the interrod gaps widened, corroborating previous studies [39, 40]. Moreover, severe DF contained additional amorphous organic matter. Nano-indentation experiments showed an homogeneous decrease in hardness by *ca*. 0.5 GPa compared to HE that was similar for mild and severe forms. The progressive increase in hardness from DEJ to enamel surface was preserved, except at the outer layer. This suggests that structural alteration occurred homogeneously over a large fraction of the enamel volume according to XRD and SEM data. These nanoindentation data also confirm an increased defect at the subsurface of enamel [41]. At the nanometer level, HR-SEM showed more homogeneous and elongated crystallite cores after etching in DF compared to HE, suggesting that the mineral phase is more stable in acidic conditions. This is in agreement with the formation of fluorapatite [42]. The presence of fluoride was confirmed by APT analysis (of the same teeth) not only in the core, but also in the shell and intergranular phase, supporting this hypothesis. PIGE studies also indicated that F accumulates at the surface of enamel, especially for severe DF. Thus, whatever the technics and the scale of analysis, higher F content was found in DF. Furthermore, thanks to specific sample preparation and use of STEM, we could observe a specific banded pattern in severe DF where local F accumulation is correlated with a highly disordered hydroxyapatite structure extending 300 nm below the enamel surface. Considering major elements of the hydroxyapatite, we observed no variation of the Ca, P content and therefore of the Ca/P ratio between the HE and DF samples. In parallel, XRD indicated that the hydroxyapatite structure and crystallites orientation were preserved although a slight broadening of the peaks was noticed. FTIR showed

that the main vibration bands of carbonated apatite were present but again with a peak broadening in DF samples. Such a broadening could reflect a loss of crystallinity which can be related to partial F incorporation [43]. Concerning the outer layer, an altered morphology and enhanced roughness of crystal surfaces have been previously reported [44].

In MIH samples, at the microstructural level observed by SEM, enamel exhibited an amorphous-like layer containing small and thinner crystallites, in accordance with prior observations [45] [46]. This structureless layer occurred both within the prisms but also in the prism sheaths. This observation is similar to the one earlier reported in a experimental model of hypomineralization considered as an organic layer [18] [24]. ATR-FTIR data showed no modification of the atomic-scale structure of apatite and only severe forms displayed amide bands indicative of the occurrence of a significant protein fraction. XRD confirmed that the crystallinity of the mineral phase was not modified and that an amorphous material was present in significant amount in severe MIH. These results are in accordance with the previously reported increased level of albumin and other proteins in MIH lesions that prevent total enamel mineralization [24-26]. This feature is specific of MIH and enamel hypomineralization resulting from similar causal factors.

The hypomineralized ‘affected enamel’ extended from the dentin-enamel junction toward the enamel surface but the loss of hardness was larger in the middle layer of enamel and for severe forms, in accordance with the literature [47] [48]. SEM highlighted that acid treatment leads to crystallites with varying external shape and core dimensions. This indicates that, in MIH lesions, mineral particles may be more soluble than in HE. In this context, APT did not indicate a clear difference in trace element concentration apart from a higher Na content, also measured by EDX, which may influence hydroxyapatite solubility. In parallel, higher levels of F were found in enamel surface compared to HE.

Noticeably, in severe DF, Fe was found at the surface using PIXE technique, also in the bulk and in the crystalline core of lesional enamel using ICP-MS and APT analyses. These findings

suggest that despite structural differences between human teeth and rodent incisors, Fe is present during dental development in both species, with exposure to fluoride able to disrupt iron metabolism [17]. Fe levels were also higher at the surface and in the bulk of MIH compared to HE whereas APT did not detect Fe in the crystallite, indicating that it could be preferentially bound by organics. Interestingly, Zn was detected on the surface of MIH enamel but not in the bulk lesions. The role of Zn in dental development and pathogenesis is unclear. Although presence of Zn on enamel surface is a common observation reflecting the diet, nutritional and environmental history of the individuals, its excess may be related to the caries development associated with MIH lesions [49] [50]. The fact that albumin is an important transporter of essential metal ions, like Cu^{2+} and Zn^{2+}, offers another explanation for this observation [51].

To sum up our micro- to nano-scale investigations of HE and DDE, we found ultrastructural, mechanical and molecular signatures in all our samples without exception:

- Rough and large enamel crystallites signify DF, while the amorphous organic layer hiding the prismatic enamel ultrastructure signs MIH.

- Weak mechanical properties deep in the enamel sign MIH, whereas reduced hardness of outer enamel layer is the sign of DF.

- The presence of a clear amide band in the FTIR spectrum is the signature of severe MIH.

Moreover, we highlighted that:

- High Fluoride content has been reported in DF (in many studies). Here, we also found high fluoride content in some MIH samples.

- Interestingly, Fe and Zn were found in both pathologies which is a characteristic of lesional enamel.

Thus, despite the different scales of analyses, these features as a whole sign a DDE. However, it should be noticed that not finding such pathognomonic signs doesn't allow to make a diagnosis of exclusion.

The structural and chemical micro- to nanoscale characteristics of HE and DDE could be, to some extent, connected to their colorimetric parameters. It should be noticed first that the analysis of colorimetric parameters showed that despite a similar range of clinical discoloration in DF and MIH, the lightness (*L**) and levels of yellow and blue (*b**) and green and red (*a**) were specific for each DDE, and also distinct from HE, except for some mild MIH samples. In normal teeth, lightness is mainly due to light scattering by HA crystals in the enamel layer whereas its color is usually mainly attributed to organic substances in dentine and DEJ [52]. Increasing porosity in enamel increases its scattering efficiency, leading to white spots with high *L**, as observed for mild DF [53]. However, when HA looses its crystallinity and organization, as observed here by SEM, HR-TEM, STEM and XRD for severe DF, scattering efficiency is expected to decrease, explaining the low *L**. In mild MIH, *L** was not significantly impacted but it decreased for severe MIH, which can be attributed to the presence of the organic phase detected here by SEM and ATR-FITR, and also by others [14, 24, 25]. Color parameters were more difficult to analyze because they combine chemical (*i.e.* the presence of colored substance such as proteins and Fe detected here by ICP-MS and APT, and physical (such as diffusion or scattering) optical phenomena. In that sense, the decrease in *a** and *b** for both mild DF and MIH could, to some extent, be correlated with the increase in *L**. In severe forms, teeth were more yellow-brown (*i.e*. higher *a** and *b**) for MIH and more red (*i.e* higher *a** but similar *b**) for DF. While the former could be related to the presence of organic matter especially proteins, the presence of additional chromophores or trace metal ions could also account for these variations. For instance, here, Fe was found in higher amounts in severe forms of both DDE and is known to provide a reddish brown coloration in pigmented enamel.

Altogether, correlation between the gathered structural and chemical information and the optical properties are not straightforward and further investigations, especially using model systems, must be considered in the future. Moreover, an important limitation of our approach is that the same sample cannot be analyzed by all techniques, mainly because many of these methods are

destructive. Moreover, nanoscale analyses, such as APT or STEM, only provide local information with a significant risk of not being representative of the whole defect, especially in the case of heterogeneous samples. Therefore, whereas our approach can provide information at different scales, it does not allow for establishing a direct connection between these scales. This can explain the observed difference in elemental composition obtained from PIGE, EDX and APT. Nevertheless, it can be noticed that high levels of F were consistently reported by these techniques in agreement with the initial clinical diagnosis of severe DDE.

4.2 Clinical significance

Altogether, while both DF and MIH involve a reduction of the mineral content of enamel, altering its structure and chemical composition, these alterations can assume very distinct forms, which also depend on the severity of the lesion. The correct diagnosis is therefore essential to determine the most adequate treatment. Currently, chemical or drug treatments to prevent DDE are unknown. In parallel, the absence of detailed knowledge of the nature and composition of lesions leads to the current use of “generalist” treatments. In the case of colored lesions, a standard protocol involves global tooth whitening, deproteinization using sodium hypochlorite, acid etching, high penetration coefficient-resin infiltration to fill the porous lesions and the use of an opaque composite [54] [35]. However, in some severe cases, the color masking is not complete after the discoloration step by hypochlorite while resin diffusion and composite bonding to enamel are unsatisfactory [10]. Our results show that for both DDE coloration may also be due to inorganic elements, that may be withdrawn using metal chelators. Differences in microstructure between DF and MIH lesions, which impact their mechanical properties, suggest that the choice of most suitable resin and composite should be DDE specific. In particular, our data suggest that there is a strong need for new low-viscosity resins to facilitate the penetration in MIH lesions due to their deep localization in order to avoid excessive removal of enamel. Finally, we found that hydroxyapatite in DF has an increased stability in acidic conditions that must be taken into account to improve the enamel-biomaterial interface for optimal composite bonding.

Recently, a new index for the diagnosis of DDE based on visual observation and tooth sensitivity was inserted in guidelines for practitioners [55]. As reported here, the spectrophotometric method that is able to discriminate between DDE and HE, and between DF and MIH lesions, could further improve diagnosis. For a clinical application, it could be adapted to each patient's anterior teeth based on the comparison of the colour parameters of lesions and HE. In particular, our results suggest that variation in *a** can be correlated to DDE severity, whereas high *b* values would indicate severe MIH. Noticeably, in the case of the presence of both DDE on a same tooth, the differential diagnosis of each defect would remain possible if they are well separated but in case of merging defects colorimetric parameters would be unpredictable.

However, several limitations of the current study must be considered. First, the possible sex and age difference in color of HE and DDE was not investigated. However, it can be noticed that the colorimetric parameters of HE of patients aged from 9 to 25 years were all included in a quite homogeneous centroid (Figure 1B) with no clear distinction between males and females. Second, samples were classified according the clinical diagnosis without taking into account the levels of exposure to the different causal factors leading to DDE. Altogether, a larger study is now necessary to further explore the variations of DDE colorimetric parameters in relation with age, sex, ethnicity and susceptibility to causal factors.

Declaration of interests

The authors declare that they have no known competing financial interests or personal relationships that could have appeared to influence the work reported in this paper.

Acknowledgments

The authors acknowledge the financial support of INSERM, IDEX Université Paris Cité and FHU-DDS-ParisNet.

The authors thank the IMPMC spectroscopy platform and O. Beyssac for his assistance with the Raman spectrometer, C. Malliakas and R. Sponenburg for technical support and all the dentists who contributed to patients' recruitment or sample donation: Dr Alfredo E. Natera (Carabobo, Venezuela), Dr Tidiane Diallo (Dakar, Senegal) and Dr Romain Jacq (Paris, France). Assistance Publique – Hôpitaux de Paris (Direction de la Recherche Clinique et de l'Innovation) was a sponsor of this study.

Funding

This project was supported by the IDEX Université Paris Cité (project FLUOREMAIL) and the EU Horizon 2020 research and innovation programme under grant agreement No. 823717 – ESTEEM3. This work was also supported in part by the National Institute of Health–National Institute of Dental and Craniofacial Research (NIH-NIDCR R01 DE025702-01). This work made use of the following core facilities operated by Northwestern University: NUCAPT, which received support from NSF (DMR-0420532), ONR (N00014-0400798, N00014-0610539, N00014-0910781 and N00014-1712870), and the Initiative for Sustainability and Energy at Northwestern University (ISEN); MatCI; NUANCE and EPIC, which received support from the International Institute for Nanotechnology (IIN), the Keck Foundation, and the State of Illinois, through the IIN; IMSERC; QBIC, which received support from NASA Ames Research Center (NNA06CB93G). NUCAPT, MatCI, NUANCE and EPIC were further supported by the MRSEC programme (NSF DMR-1720139) at the Materials Research Center; NUCAPT, NUANCE, EPIC and IMSERC were also supported by the Soft and Hybrid Nanotechnology Experimental (SHyNE) Resource (NSF ECCS-1542205).

References

[1] S.J. AlQahtani, M.P. Hector, H.M. Liversidge, Brief communication: The London atlas of human tooth development and eruption, Am J Phys Anthropol 142(3) (2010) 481-90.
[2] R.S. Lacruz, S. Habelitz, J.T. Wright, M.L. Paine, Dental Enamel Formation and Implications for Oral Health and Disease, Physiol Rev 97(3) (2017) 939-993.
[3] F. Mohabatpour, X. Chen, S. Papagerakis, P. Papagerakis, Novel trends, challenges and new perspectives for enamel repair and regeneration to treat dental defects, Biomater Sci 10(12) (2022) 3062-3087.
[4] O. Fejerskov, M.J. Larsen, A. Richards, V. Baelum, Dental tissue effects of fluoride, Adv Dent Res 8(1) (1994) 15-31.
[5] K. Elhennawy, F. Schwendicke, Managing molar-incisor hypomineralization: A systematic review, J Dent 55 (2016) 16-24.
[6] A. Rasool, A. Farooqi, T. Xiao, W. Ali, S. Noor, O. Abiola, S. Ali, W. Nasim, A review of global outlook on fluoride contamination in groundwater with prominence on the Pakistan current situation, Environmental geochemistry and health 40(4) (2018) 1265-1281.
[7] D. Zhao, B. Dong, D. Yu, Q. Ren, Y. Sun, The prevalence of molar incisor hypomineralization: evidence from 70 studies, Int J Paediatr Dent 28(2) (2018) 170-179.
[8] F. Schwendicke, K. Elhennawy, S. Reda, K. Bekes, D.J. Manton, J. Krois, Global burden of molar incisor hypomineralization, J Dent 68 (2018) 10-18.
[9] A.B. Borges, T.M. Caneppele, D. Masterson, L.C. Maia, Is resin infiltration an effective esthetic treatment for enamel development defects and white spot lesions? A systematic review, J Dent 56 (2017) 11-18.
[10] M. Lagarde, E. Vennat, J.P. Attal, E. Dursun, Strategies to optimize bonding of adhesive materials to molar-incisor hypomineralization-affected enamel: A systematic review, Int J Paediatr Dent 30(4) (2020) 405-420.
[11] T. Aoba, O. Fejerskov, Dental fluorosis: chemistry and biology, Crit Rev Oral Biol Med 13(2) (2002) 155-70.
[12] M.A.R. Buzalaf, Review of Fluoride Intake and Appropriateness of Current Guidelines, Adv Dent Res 29(2) (2018) 157-166.
[13] A.L. Bronckers, D.M. Lyaruu, P.K. DenBesten, The impact of fluoride on ameloblasts and the mechanisms of enamel fluorosis, J Dent Res 88(10) (2009) 877-93.
[14] E.C. Moreno, M. Kresak, R.T. Zahradnik, Fluoridated hydroxyapatite solubility and caries formation, Nature 247(5435) (1974) 64-5.
[15] S. Houari, T. Wurtz, D. Ferbus, D. Chateau, A. Dessombz, A. Berdal, S. Babajko, Asporin and the mineralization process in fluoride-treated rats, J Bone Miner Res 29(6) (2014) 1446-55.
[16] J. Li, P. Wang, J. Gao, X. Fei, Y. Liu, J. Ruan, NaF Reduces KLK4 Gene Expression by Decreasing Foxo1 in LS8 Cells, Biol Trace Elem Res 186(2) (2018) 498-504.
[17] S. Houari, E. Picard, T. Wurtz, E. Vennat, N. Roubier, T.D. Wu, J.L. Guerquin-Kern, M. Duttine, T.T. Thuy, A. Berdal, S. Babajko, Disrupted Iron Storage in Dental Fluorosis, J Dent Res 98(9) (2019) 994-1001.
[18] K. Jedeon, S. Houari, S. Loiodice, T.T. Thuy, M. Le Normand, A. Berdal, S. Babajko, Chronic Exposure to Bisphenol A Exacerbates Dental Fluorosis in Growing Rats, J Bone Miner Res 31(11) (2016) 1955-1966.
[19] H. Dong, X. Yang, S. Zhang, X. Wang, C. Guo, X. Zhang, J. Ma, P. Niu, T. Chen, Associations of low level of fluoride exposure with dental fluorosis among U.S. children and adolescents, NHANES 2015-2016, Ecotoxicol Environ Saf 221 (2021) 112439.
[20] G.A. Leite, R.M. Sawan, J.M. Teofilo, I.M. Porto, F.B. Sousa, R.F. Gerlach, Exposure to lead exacerbates dental fluorosis, Arch Oral Biol 56(7) (2011) 695-702.

[21] J.A. Dulla, H. Meyer-Lueckel, Molar-incisor hypomineralisation: narrative review on etiology, epidemiology, diagnostics and treatment decision, Swiss Dent J 131(11) (2021).
[22] M. Bezamat, J.F. Souza, F.M.F. Silva, E.G. Correa, A.L. Fatturi, J.A. Brancher, F.M. Carvalho, T. Cavallari, L. Bertolazo, C. Machado-Souza, M. Koruyucu, M. Bayram, A. Racic, B.M. Harrison, Y.Y. Sweat, A. Letra, D. Studen-Pavlovich, F. Seymen, B. Amendt, R.I. Werneck, M.C. Costa, A. Modesto, A.R. Vieira, Gene-environment interaction in molar-incisor hypomineralization, PLoS One 16(1) (2021) e0241898.
[23] S. Alaluusua, P.L. Lukinmaa, J. Torppa, J. Tuomisto, T. Vartiainen, Developing teeth as biomarker of dioxin exposure, Lancet 353(9148) (1999) 206.
[24] K. Jedeon, M. De la Dure-Molla, S.J. Brookes, S. Loiodice, C. Marciano, J. Kirkham, M.C. Canivenc-Lavier, S. Boudalia, R. Berges, H. Harada, A. Berdal, S. Babajko, Enamel defects reflect perinatal exposure to bisphenol A, Am J Pathol 183(1) (2013) 108-18.
[25] J.E. Mangum, F.A. Crombie, N. Kilpatrick, D.J. Manton, M.J. Hubbard, Surface integrity governs the proteome of hypomineralized enamel, J Dent Res 89(10) (2010) 1160-5.
[26] V.A. Perez, J.E. Mangum, M.J. Hubbard, Pathogenesis of Molar Hypomineralisation: Aged Albumin Demarcates Chalky Regions of Hypomineralised Enamel, Front Physiol 11 (2020) 579015.
[27] P. Malmberg, J.G. Noren, D. Bernin, Molecular insights into hypomineralized enamel, Eur J Oral Sci 127(4) (2019) 340-346.
[28] W.K. Seow, Developmental defects of enamel and dentine: challenges for basic science research and clinical management, Aust Dent J 59 Suppl 1 (2014) 143-54.
[29] N. Kilpatrick, New developments in understanding development defects of enamel: optimizing clinical outcomes, J Orthod 36(4) (2009) 277-82.
[30] V. Srot, B. Bussmann, U. Salzberger, C.T. Koch, P.A. van Aken, Linking microstructure and nanochemistry in human dental tissues, Microsc Microanal 18(3) (2012) 509-23.
[31] K.A. DeRocher, P.J.M. Smeets, B.H. Goodge, M.J. Zachman, P.V. Balachandran, L. Stegbauer, M.J. Cohen, L.M. Gordon, J.M. Rondinelli, L.F. Kourkoutis, D. Joester, Chemical gradients in human enamel crystallites, Nature 583(7814) (2020) 66-71.
[32] M.N. Y. Wang, Handbook of Modern Ion Beam Materials Analysis, 2nd Edition (2010),.
[33] F. Guerra, M. Mazur, D. Corridore, D. Pasqualotto, G.M. Nardi, L. Ottolenghi, Evaluation of the esthetic properties of developmental defects of enamel: a spectrophotometric clinical study, ScientificWorldJournal 2015 (2015) 878235.
[34] K.L. Weerheijm, Molar incisor hypomineralisation (MIH), Eur J Paediatr Dent 4(3) (2003) 114-20.
[35] N.A. Lygidakis, E. Garot, C. Somani, G.D. Taylor, P. Rouas, F.S.L. Wong, Best clinical practice guidance for clinicians dealing with children presenting with molar-incisor-hypomineralisation (MIH): an updated European Academy of Paediatric Dentistry policy document, Eur Arch Paediatr Dent 23(1) (2022) 3-21.
[36] Fairchild, Color Appearance Models, (2013) 471.
[37] v.h.w.p.o. Python Software Foundation. Python Language Reference.
[38] https://docs.opencv.org/4.1.2/de/d25/imgproc_color_conversions.html.
[39] B. Kerebel, G. Daculsi, [Ultrastructural and crystallographic study of human enamel in endemic fluorosis], J Biol Buccale 4(2) (1976) 143-54.
[40] T. Yanagisawa, S. Takuma, O. Fejerskov, Ultrastructure and composition of enamel in human dental fluorosis, Adv Dent Res 3(2) (1989) 203-10.
[41] J. Min, P. Yu, Z. Xu, Z. Li, Q. Zhang, H. Yu, S. Gao, Investigation on the Gradient Nanomechanical Behavior of Dental Fluorosis Enamel, Nanoscale Res Lett 13(1) (2018) 347.
[42] C. Robinson, S. Connell, J. Kirkham, S.J. Brookes, R.C. Shore, A.M. Smith, The effect of fluoride on the developing tooth, Caries Res 38(3) (2004) 268-76.

[43] V. Zavala-Alonso, J.P. Loyola-Rodriguez, H. Terrones, N. Patino-Marin, G.A. Martinez-Castanon, K. Anusavice, Analysis of the molecular structure of human enamel with fluorosis using micro-Raman spectroscopy, J Oral Sci 54(1) (2012) 93-8.
[44] E.K. Mahoney, R. Rohanizadeh, F.S. Ismail, N.M. Kilpatrick, M.V. Swain, Mechanical properties and microstructure of hypomineralised enamel of permanent teeth, Biomaterials 25(20) (2004) 5091-100.
[45] T.G. Fagrell, W. Dietz, B. Jalevik, J.G. Noren, Chemical, mechanical and morphological properties of hypomineralized enamel of permanent first molars, Acta Odontol Scand 68(4) (2010) 215-22.
[46] T. Fagrell, Molar incisor hypomineralization. Morphological and chemical aspects, onset and possible etiological factors, Swed Dent J Suppl (216) (2011) 5, 11-83.
[47] G.W. Suckling, D.G. Nelson, M.J. Patel, Macroscopic and scanning electron microscopic appearance and hardness values of developmental defects in human permanent tooth enamel, Adv Dent Res 3(2) (1989) 219-33.
[48] Z.H. Xie, E.K. Mahoney, N.M. Kilpatrick, M.V. Swain, M. Hoffman, On the structure-property relationship of sound and hypomineralized enamel, Acta Biomater 3(6) (2007) 865-72.
[49] J.A. Grossi, R.N. Cabral, S.C. Leal, Caries Experience in Children with and without Molar-Incisor Hypomineralisation: A Case-Control Study, Caries Res 51(4) (2017) 419-424.
[50] M.T. Rahman, A. Hossain, C.H. Pin, N.A. Yahya, Zinc and Metallothionein in the Development and Progression of Dental Caries, Biol Trace Elem Res 187(1) (2019) 51-58.
[51] I. Petitpas, C.E. Petersen, C.E. Ha, A.A. Bhattacharya, P.A. Zunszain, J. Ghuman, N.V. Bhagavan, S. Curry, Structural basis of albumin-thyroxine interactions and familial dysalbuminemic hyperthyroxinemia, Proc Natl Acad Sci U S A 100(11) (2003) 6440-5.
[52] A. Joiner, Tooth colour: a review of the literature, J Dent 32 Suppl 1 (2004) 3-12.
[53] M. Denis, A. Atlan, E. Vennat, G. Tirlet, J.P. Attal, White defects on enamel: diagnosis and anatomopathology: two essential factors for proper treatment (part 1), Int Orthod 11(2) (2013) 139-65.
[54] O. Marouane, N. Douki, F. Chtioui, A Combined Approach for the Aesthetic Management of Stained Enamel Opacities: External Bleaching Followed by Resin Infiltration, Case Rep Dent 2018 (2018) 1605842.
[55] R. Steffen, N. Kramer, K. Bekes, The Wurzburg MIH concept: the MIH treatment need index (MIH TNI) : A new index to assess and plan treatment in patients with molar incisior hypomineralisation (MIH), Eur Arch Paediatr Dent 18(5) (2017) 355-361.

Figure captions

Figure 1 : DDE digital tooth color measurements. A Photographs of anterior teeth representative of each pathology according to the severity classification compared to healthy ones from control patients. Spectrophotometer pictures of representative teeth. Detailed color maps provided by the Spectroshade MHT® based on the analog VITA 3D MASTER shade guide. **B** Point cloud representation of *L*a*b** coordinates in CIELab color space of each of the teeth analysed. The main 3D representation is surrounded by a red ellipse. Each small dot represents the average color coordinates for a selected area on a tooth and each bigger dot represents the centroid of one analysis condition. Projections onto the L*a*, L*b*, and a*b* planes (green ellipses) are additionally drawn to better visualize the distributions.

Figure 2: DDE mechanical properties. A Enamel hardness as a function of distance from the dentin-enamel junction (DEJ) to the surface (µm), comparing healthy enamel (HE) (control patients) with enamel from patients with mild and severe fluorosis. **B** Enamel Hardness as a function of distance from the DEJ to the enamel external surface, comparing unaffected areas**,** mild and severe MIH lesions. Inner (first 100 µm), middle, and outer enamel (last 100 µm) layers are delimitated by dashed lines.

Figure 3: DDE ultrastructure by Electron Microscopy. A Representative images of each condition. **B** SEM images of sections through the outer layer of enamel lesions compared to the healthy enamel. Rod and interrod (IR) enamel are indicated by dotted green and black lines respectively. **C** SEM images of sections showing enamel crystallites in healthy enamel (33) and enamel lesions. White arrows indicate where preferential dissolution of the crystallite core resulted in formation of hollow crystallites. Scale bar: 100 nm. **D 1.** Macroscopic view of surface enamel from a tooth with severe DF. Scale bar: 2 mm. **2.** BF-STEM images from light band (left) showing “normal” enamel (NE) and a dark band (right) showing a “shattered area” (SA) underneath followed by NE. Scale bar: 100 nm. **3.** HR-TEM images from light band (left) and dark band (right). Scale bar: 50 nm. **4.** HAADF-STEM image visualizing from the surface to ≅ 2 µm deep into the enamel. Scale bar: 500 nm. **5.** Bar plot of mean atomic fractions of F and Na, and of the ratio of the atomic fractions of calcium over that of phosphorous (Ca/P) for each zone, as assessed using STEM-EDX. Zone 1 corresponds to the SA. n = 6 measurements/zone on 2 different teeth.

Figure 4: Crystallographic and spectroscopic characterizations of DDE. A X-ray diffraction patterns of each condition. Miller indices for hydroxyapatite reflections are provided above the sample labeled ‘control enamel’ (black line). The diffractograms have been normalized to the intensity of the most intense Bragg peak and have been vertically shifted by an arbitrary value to allow their comparison. n=2 enamel samples/condition of severity. **B** Optical image of a severe DF sample used for the 2D diffraction experiment (scale bar: 100 µm) containing an affected region (1), a transitional region (2) and an unaffected region (3). Diffraction data on 2 different points for each region (marked with a star *) were collected and averaged. One-dimensional diffraction patterns after integrating the 2D diffraction data. **C1** ATR-FTIR spectra of Healthy Enamel (HE) (black line A) compared to mild DF (orange line B), severe DF (red line C), mild MIH (light green line D) and severe MIH (dark green line E). **C2** Region of the ATR-FTIR spectra showing the v_2CO_3 bands. **C3** Region of the ATR-FTIR spectra showing the v_3CO_3 bands. Spectra were multiplied by an arbitrary scale factor (indicated on the right) and shifted vertically to facilitate their comparison.

Figure 5: DDE chemical composition. A Plot of mass fraction of F, Na and P on the outer surface of enamel, as assessed by PIGE. n= 2 to 4 measurement points on 2 different samples/condition. **B** Plot of mass fraction of Ca, Na, P and Mg in the lesion body, using ICP-OES. Ca/P ratios were calculated from mass fractions. n= 2 samples/condition. **C** Mass fraction of trace elements Fe and Zn measured on the outer surface of enamel by PIXE. n= 4 measurement points on 2 different samples/condition. **D** Mass fraction of trace elements Fe and Zn measured in the body of the lesion by ICP-MS. n= 2 samples/condition. Note that for all plots but for the Ca/P ratio, the decadic logarithm of the mass fraction (in ppm) is given.

Figure 6: Atomic-scale DDE structure and composition. APT 3D reconstructions of (**A)** mild MIH enamel, (**B**) severe MIH enamel, (**C**) mild DF enamel, (**D**) severe DF enamel, and (**E**) healthy enamel for comparison (33) with intergranular (ig), shell (sh) and core (co) regions of crystallites indicated. **1.** Mg distribution. **2.** Na distribution. **3.** F distribution. **4.** Carbonyl (COH) distribution, **5.** 1D concentration profile elucidates the distribution of ions across a crystallite. Scale bars: (A – D) 20 nm, (E) 30 nm. n= 16 tips for MIH from 2 patients and 13 tips for DF from 2 patients.

Figure 1

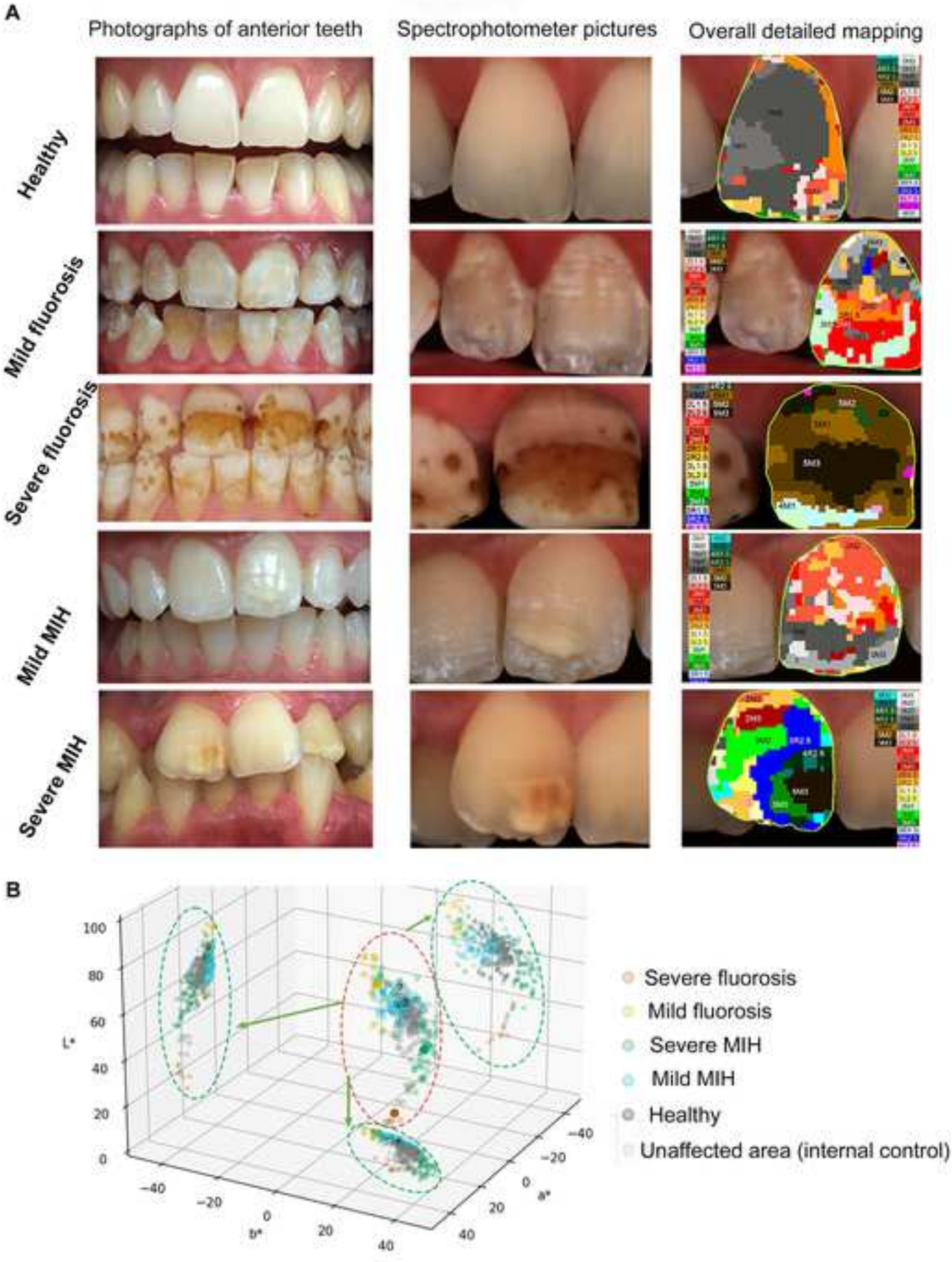

Figure 2

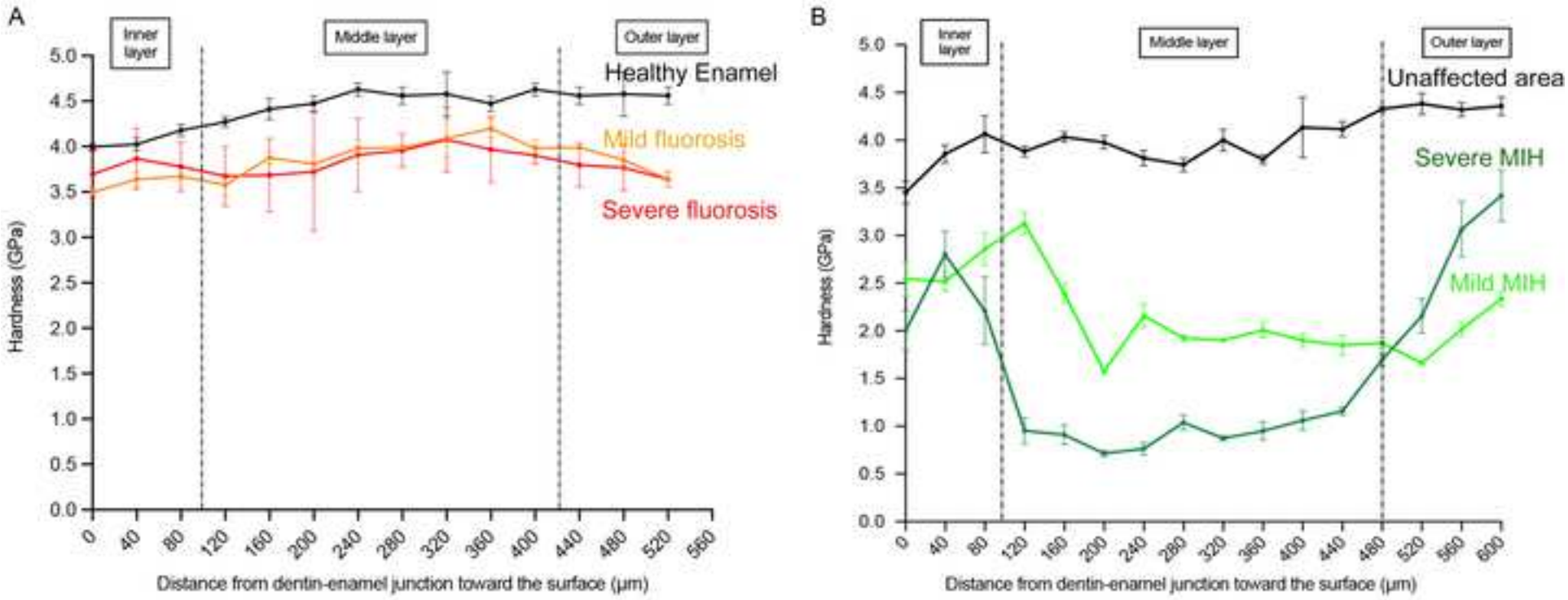

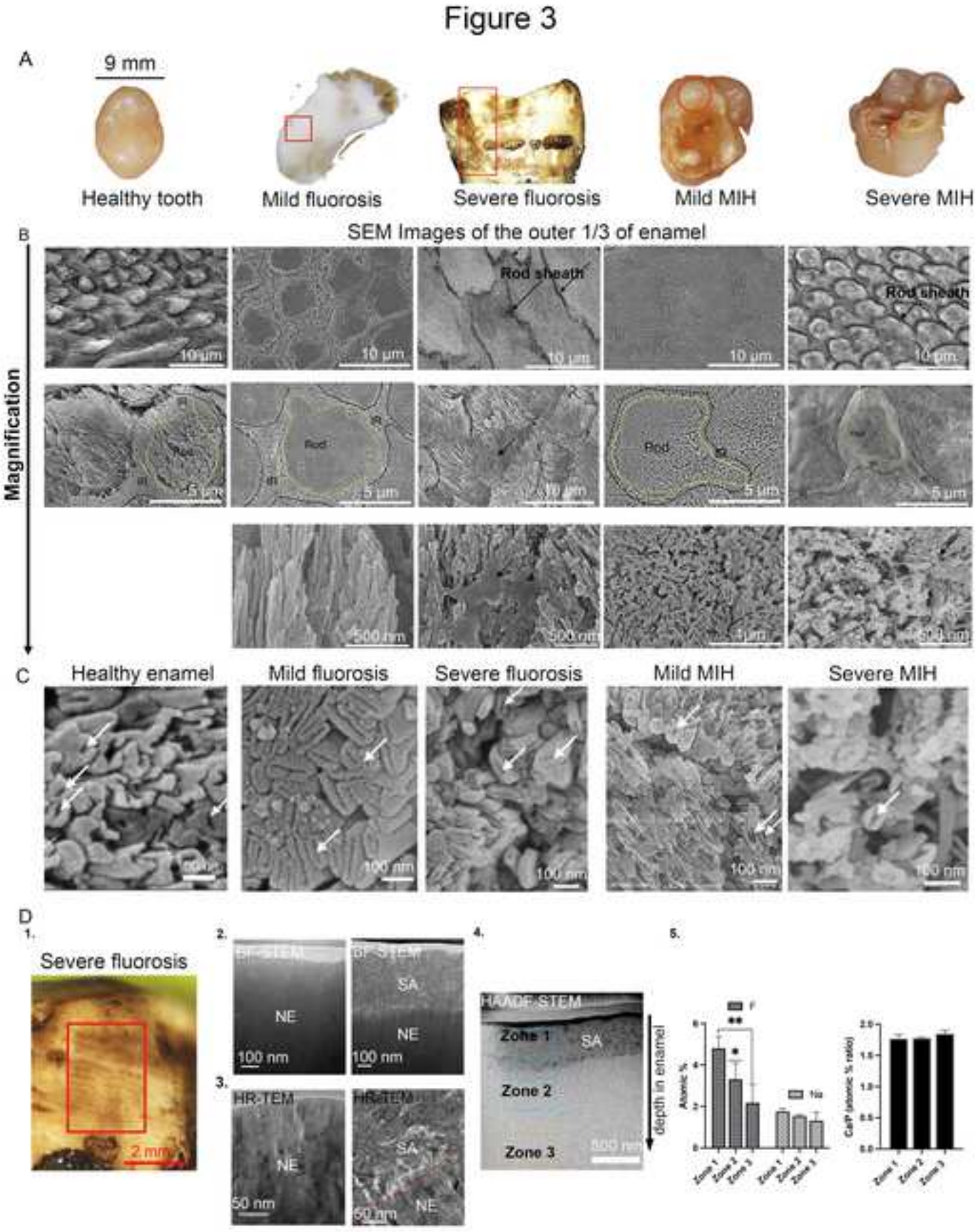
Figure 3
A
9 mm
Healthy tooth
Mild fluorosis
Severe fluorosis
Mild MIH
Severe MIH
B
SEM Images of the outer 1/3 of enamel
Magnification
Rod sheath
Rod
C
Healthy enamel
Mild fluorosis
Severe fluorosis
Mild MIH
Severe MIH
D
1.
Severe fluorosis
2 mm
2.
NE
SA
100 nm
3.
HR-TEM
50 nm
60 nm
4.
HAADF-STEM
Zone 1
Zone 2
Zone 3
depth in enamel
5.
Atomic %
Ca/P (atomic % ratio)

Figure 4

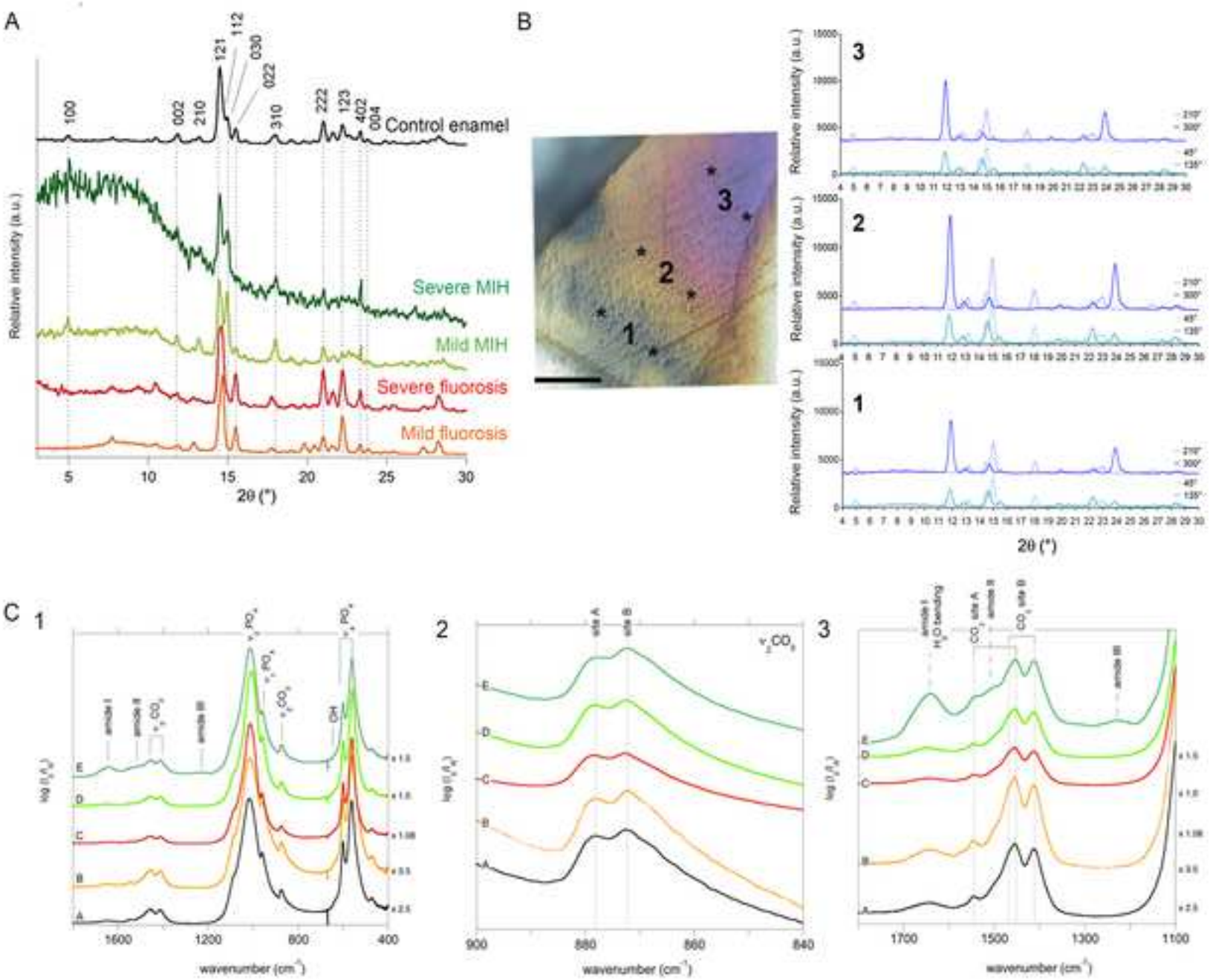

Figure 5

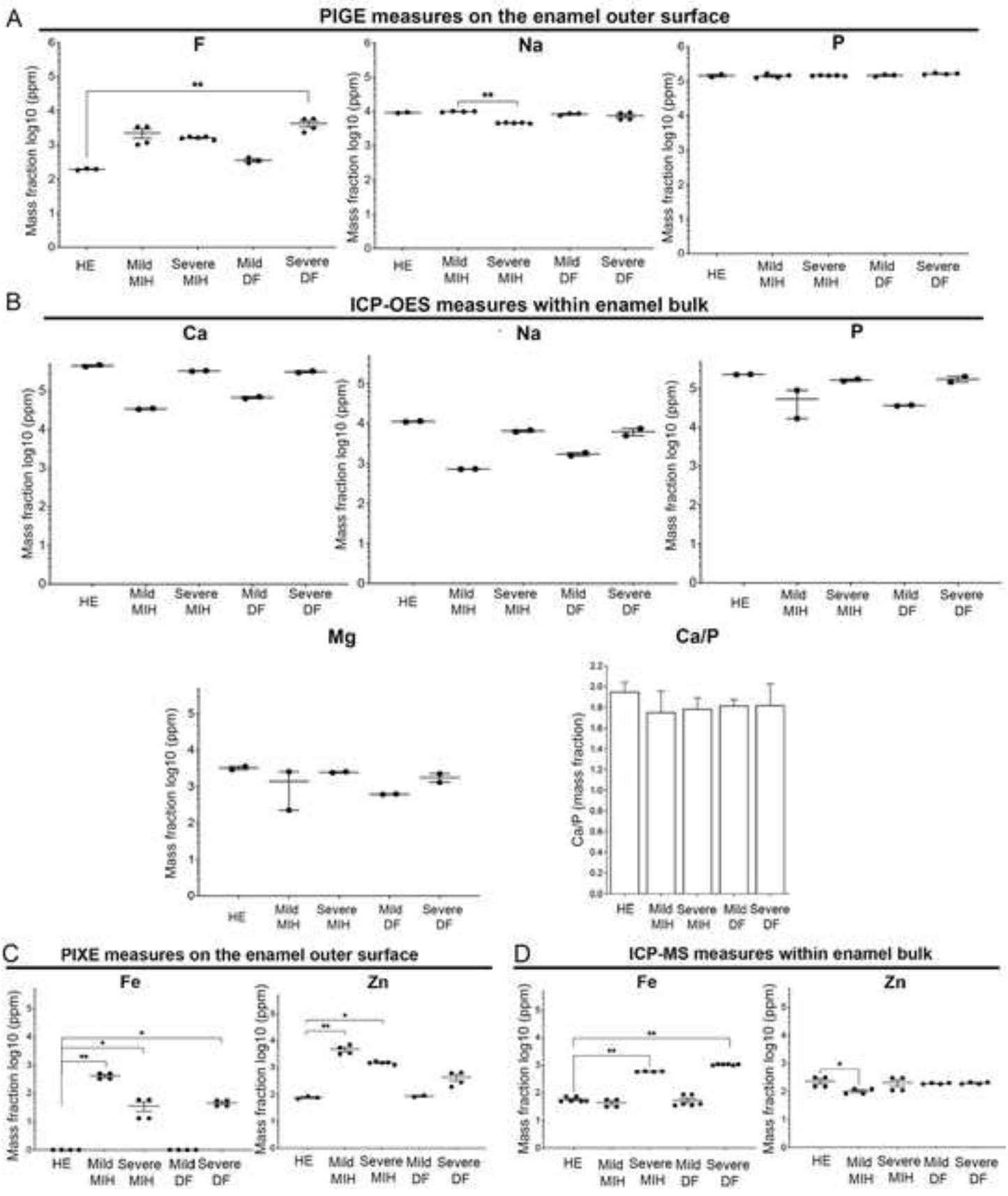

Figure 6

Click here to access/download;Figure(s);Figure 6.tif

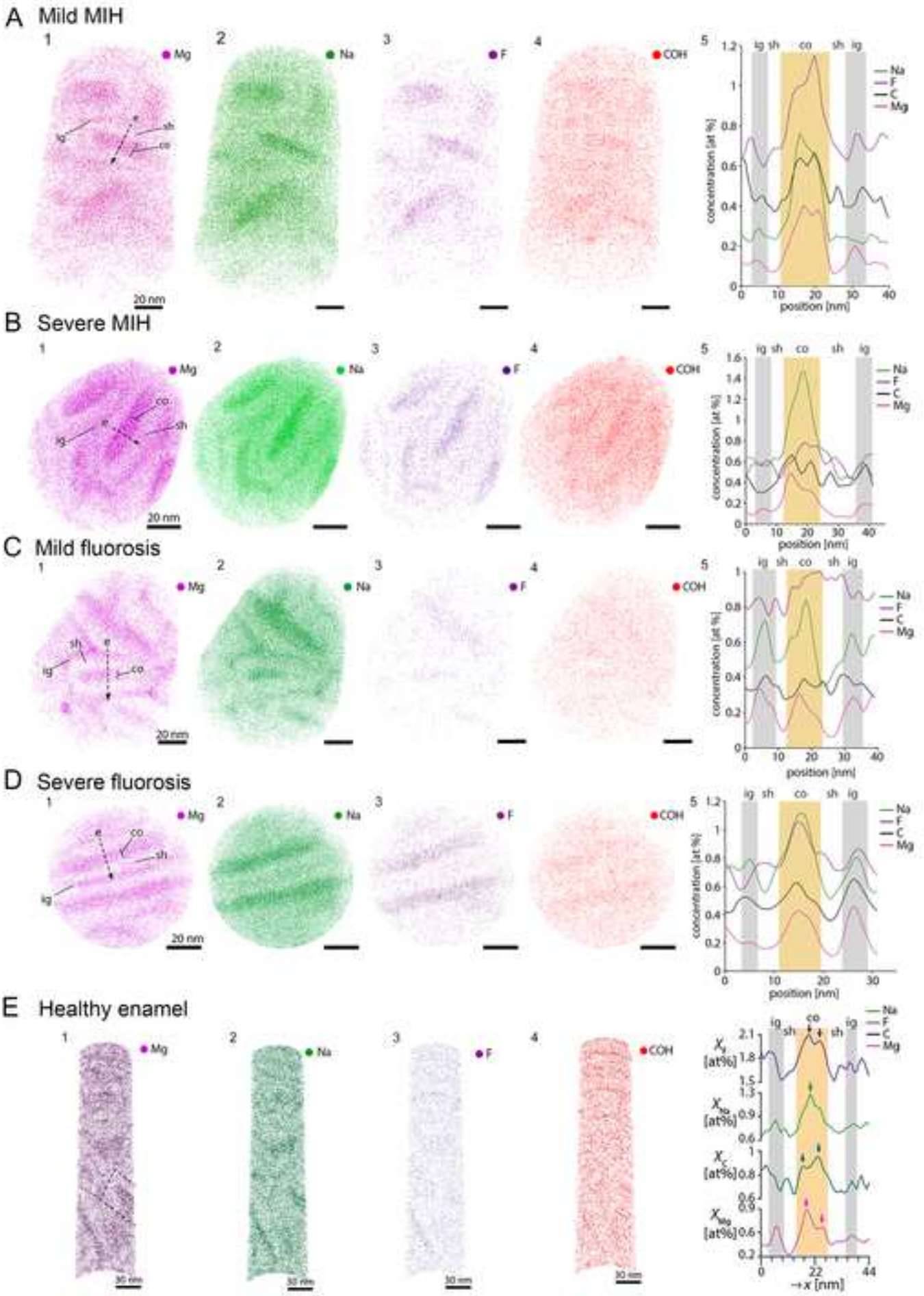

Table 1. Overview of the samples used in this study for each technique. ua = unaffected area, M = molar, PM = premolar, I = incisor.

Techniques	Developmental Defect of Enamel				Healthy Enamel
	MIH		DF		
	Mild	Severe	Mild	Severe	
Spectrophotometry	42 patients 120 teeth 45 ua		32 patients 94 teeth -		15 patients 21 teeth -
SEM	M1 M2	M6 M7	M8 M9	M11 M12	PM1 PM2
STEM & HR-TEM	M3	M6	M10	M11 M12	- -
Nanoindentation	M5		I9 I10	I14 M13	I16 -
XRD	M4 I3 I4	M7 I5 I6	I11 I12 M8	I15 M14 -	M17 PM2 ua M1
FTIR	M3 I1 I2	M6 I3 I4	M10 I13	M11 M15 M16	PM1 ua M2 ua M3
PIGE-PIXE	M3 I1 I2	M6 I7 I8	M10 I13	M11 M12 M13	PM1 ua M2 ua M3
ICP-MS/OES	M4 I3 I4	M7 I5 I6	I11 I12 M10	I15 M14 -	M17 PM2 uaM1
APT	M1 (4 tips) M2 (4 tips)	M6 (4 tips) M7 (4 tips)	M8 (2 tips) M9 (3 tips)	M11 (4 tips) M12 (4 tips)	*De Rocher et al.2020*

Declaration of interests

☒ The authors declare that they have no known competing financial interests or personal relationships that could have appeared to influence the work reported in this paper.

☐The authors declare the following financial interests/personal relationships which may be considered as potential competing interests: